EFEMP1 contributes to light-dependent ocular growth in zebrafish

Jiaheng Xie[1], Bang V. Bui[2], Patrick T. Goodbourn[3], Patricia R. Jusuf[1]*

[1] School of Biosciences, The University of Melbourne
[2] Department of Optometry and Vision Sciences, The University of Melbourne
[3] Melbourne School of Psychological Sciences, The University of Melbourne
*patricia.jusuf@unimelb.edu.au

Abstract

Myopia (short-sightedness) is the most common ocular disorder. It generally develops after over-exposure to aberrant visual environments, disrupting emmetropization mechanisms that should match eye growth with optical power. A pre-screening of strongly associated myopia-risk genes identified through human genome-wide association studies implicates *efemp1* in myopia development, but how this gene impacts ocular growth remains unclear. Here, we modify *efemp1* expression specifically in the retina of zebrafish. We found that under normal lighting, *efemp1* mutants developed axial myopia, enlarged eyes, reduced spatial vision and altered retinal function. However, under myopia-inducing dark-rearing, compared to control fish, mutants remained emmetropic and showed changes in retinal function. *Efemp1* modification changed the expression of *efemp1*, *egr1*, *tgfb1a*, *vegfab* and *rbp3* genes in the eye, and changes the inner retinal distributions of myopia-associated EFEMP1, TIMP2 and MMP2 proteins. *Efemp1* modification also impacted dark-rearing-induced responses of *vegfab* and *wnt2b* genes and above-mentioned myopia-associated proteins. Together, we provided robust evidence that light-dependent ocular growth is regulated by *efemp1*.

Summary

This study shows that retina-specific modification of *efemp1* expression in zebrafish results in myopic eye, and impacts responses to myopia-inducing dark-rearing in eye growth, retinal function, and myopia-associated molecular expression and distribution, implicating light-dependent regulation of *efemp1* in ocular development.

Introduction

Myopia (short-sightedness) is now the most common visual disorder, and is predicted to impact approximately half of the world population by 2050 (Holden et al., 2016). Although considered manageable with optical correction, the development of high levels of myopia (or pathological myopia) brings with it ocular changes that promote retinal disease that cannot be easily managed. Thus, there is an urgent need to better understand this condition.

During development, emmetropization mechanisms use visual cues to regulate eye growth, in order to match eye size with its optic power, to achieve focused vision (Rabin et al., 1981). Extended exposure to aberrant visual environments can lead to dysregulation of emmetropization mechanisms resulting in myopia. Human studies showed that children who spent more time outdoors were less likely to develop myopia (Rose et al., 2008). Recent shifts away from outdoor activities and increased screen time may further increase myopia prevalence and promote pathological myopia (Najafzadeh et al., 2023). This points to an urgent need to understand the underlying mechanisms for myopia development, to underpin the development of novel approaches to target these mechanisms.

A range of myopia-associated genes have been identified over the past several decades (Tedja et al., 2019). Meta-analyses of an increasingly large pool of human genome-wide association (GWAS) data have seen a growth in the number of novel risk genes associated with refractive error (Tedja et al., 2018). Amongst the highest ranked myopia risk genes is *EGF containing fibulin extracellular matrix protein 1* (*efemp1*). EFEMP1 is a secreted extracellular matrix glycoprotein widely expressed throughout the human body, especially in elastic fiber-rich tissues, for examples, the brain, lung, kidney and eye (Livingstone et al., 2020). In relation to visual diseases, an autosomal dominant gain-of-function mutation in the *EFEMP1* gene (c.1033C>T, p.Arg345Trp) is known to be associated with Malattia Leventinese and Doyne honeycomb retinal dystrophy (Stone et al., 1999), leading to accumulation of drusen (yellow-white deposits) beneath the basal retinal pigment epithelium (RPE), a pathologic sign that overlaps with age-related macular degeneration (AMD) (Marmorstein et al., 2002). A number of studies suggest that sub-RPE deposits may result from abnormal interactions between EFEMP1 and

complement system proteins, for example, complement component 3 (C3), complement factor B (FB) and complement factor H (CFH) (Crowley et al., 2022; Garland et al., 2013).

Recently, from 3 independent Filipino families, three novel *EFEMP1* variants (c.238A>T, p.Asn80Tyr; c.1480T>C, p.Ter494Glnext*29; and c.1429C>T, p.Arg477Cys) were identified in patients with juvenile-onset open-angle glaucoma, in which 76% of the carriers eventually developed blindness (Collantes et al., 2022). This study also demonstrated that protein aggregation and retention was the potential cause of juvenile-onset open-angle glaucoma. In addition, a recent reported case with biallelic *EFEMP1* loss-of-function variants (c.320_324del, p.Met107fs; c.615T>A, p.Tyr205Ter) manifested connective tissue abnormalities, including tall stature, hernia, hypermobile joints, thin translucent skin, and importantly high myopia (Driver et al., 2020). These clinical findings highlight a role for *EFEMP1* in ocular development, however how *efemp1* is involved in ocular refractive development remains largely unknown.

In the current study, using a zebrafish model with retina-specific *efemp1* modification, we show robust evidence that *efemp1* regulates ocular growth in a light-dependent manner in zebrafish. In particular, mutant fish developed myopia and enlarged eyes when reared under normal lighting, but became emmetropic after dark-rearing (a myopia-inducing condition for normal fish). In addition, we show that *efemp1* may mediate ocular growth by regulating expression of *early growth response 1* (*egr1*), *transforming growth factor beta 1b* (*tgfb1a*), *vascular endothelial growth factor Ab* (*vegfab*) and *retinol binding protein 3* (*rbp3*), and modulating light-dependent responses of *Wnt family 2B* (*wnt2b*) and *vegfab*. Meanwhile, retinal *efemp1* modification influences inner retinal distribution of matrix metalloproteinase 2 (MMP2) and tissue inhibitor of metalloproteinase 2 (TIMP2) for both intrinsic and visually induced ocular growth. This study demonstrates the capacity of a comprehensive zebrafish analysis platform, combining genetic and environmental manipulations, as well as multifaceted phenotypic assessments, to gain insights into GWAS-associated myopia-risk genes in myopia development.

84 ## Results

85 ### Retina-specific disruption of *efemp1* leads to reduced visual sensitivity

86 In order to investigate the role of the *efemp1* gene, we first generated a zebrafish line with retina-specific
87 *efemp1* modification (*efemp1*$^{2C\text{-}Cas9}$; Fig 1A), using a 2C-Cas9 somatic CRISPR gene editing system (Di
88 Donato et al., 2016). In this transgenic zebrafish line, Tg(*rx2*:*Gal4*) is expressed specifically in the
89 retina, due to the *retina-specific retinal homeobox gene 2* (*rx2*) promoter. The Gal4 transcription factor
90 binds the upstream activating sequence (UAS) element of the 2C-Cas9 transgene
91 Tg(*UAS*:*Cas9T2ACre*;*U6*:*efemp1sgRNA1*;*U6*:*efemp1sgRNA2*), leading to expression of the Cas9
92 nuclease and Cre recombinase. The retina-specific Cas9 nuclease then combines with universally
93 expressed *efemp1* small guide RNAs (sgRNAs), which target exons 3 and 5 of the *efemp1* genome DNA
94 (gDNA) for CRISPR gene editing in the retina (Fig 1B). The Cre recombinase recombines loxP sites in
95 the Tg(*bact2-loxP-mCherry-loxP-eGFP*) and switches mCherry to eGFP fluorophore reporter
96 specifically in the eye, thus allowing for selection of Cas9-positive mutants (Fig 1A′). This gene editing
97 system led to mosaic retinal mutations (Fig 1A′). Genetic control fish (*efemp1*$^{+/+}$) had the same
98 transgenic background except that they lacked the 2C-Cas9 transgene.

99 We used headloop PCR, which specifically suppresses amplification of wildtype (unmutated) DNA
100 sequences containing sgRNA target sites, but allows targeted mutant sequences to undergo normal PCR
101 amplification. We showed that there were discernibly higher amounts of PCR products amplified from
102 30 ng of *efemp1*$^{2C\text{-}Cas9}$ eye gDNA than from 30 ng of control eye gDNA for both target sites,
103 demonstrating that there were mutations in the mutant zebrafish retina (Fig 1C–D). However, the
104 headloop PCR bands of *efemp1*$^{2C\text{-}cas9}$ fish were remarkably weaker than standard PCR bands, suggesting
105 a low mutation rate. This may have arisen as our gDNA was extracted from whole zebrafish eyes rather
106 than just the retina or Cas9+ cells.

107 Our preliminary data showed that 5 days post-fertilization (dpf) fish with *efemp1* knockdown by
108 morpholino presented reduced spatial-frequency tuning functions (unpublished). Therefore, we tested
109 optomotor responses (OMR) for our mutant fish to verify modification of *efemp1* at the behavioral level.
110 Our 5 dpf *efemp1*$^{2C\text{-}Cas9}$ mutants showed altered spatial-frequency tuning functions ($P = 0.0334$; Fig 1E),

111 with a significant amplitude reduction (*P = 0.0412*; Fig 1F) in *efemp1*$^{2C\text{-}Cas9}$ fish. There was no
112 difference in peak spatial frequency (Fig 1G) and function bandwidth (Fig 1H) between genotypes.
113 OMR assessment at 2 weeks post-fertilization (wpf) returned similar differences between mutants and
114 their wildtype counterparts (spatial-frequency tuning function: *P = 0.0034*; amplitude: *P = 0.0022*; Fig
115 S1). Taken together, *efemp1*$^{2C\text{-}Cas9}$ fish are a robust model of retinal *efemp1* modification.

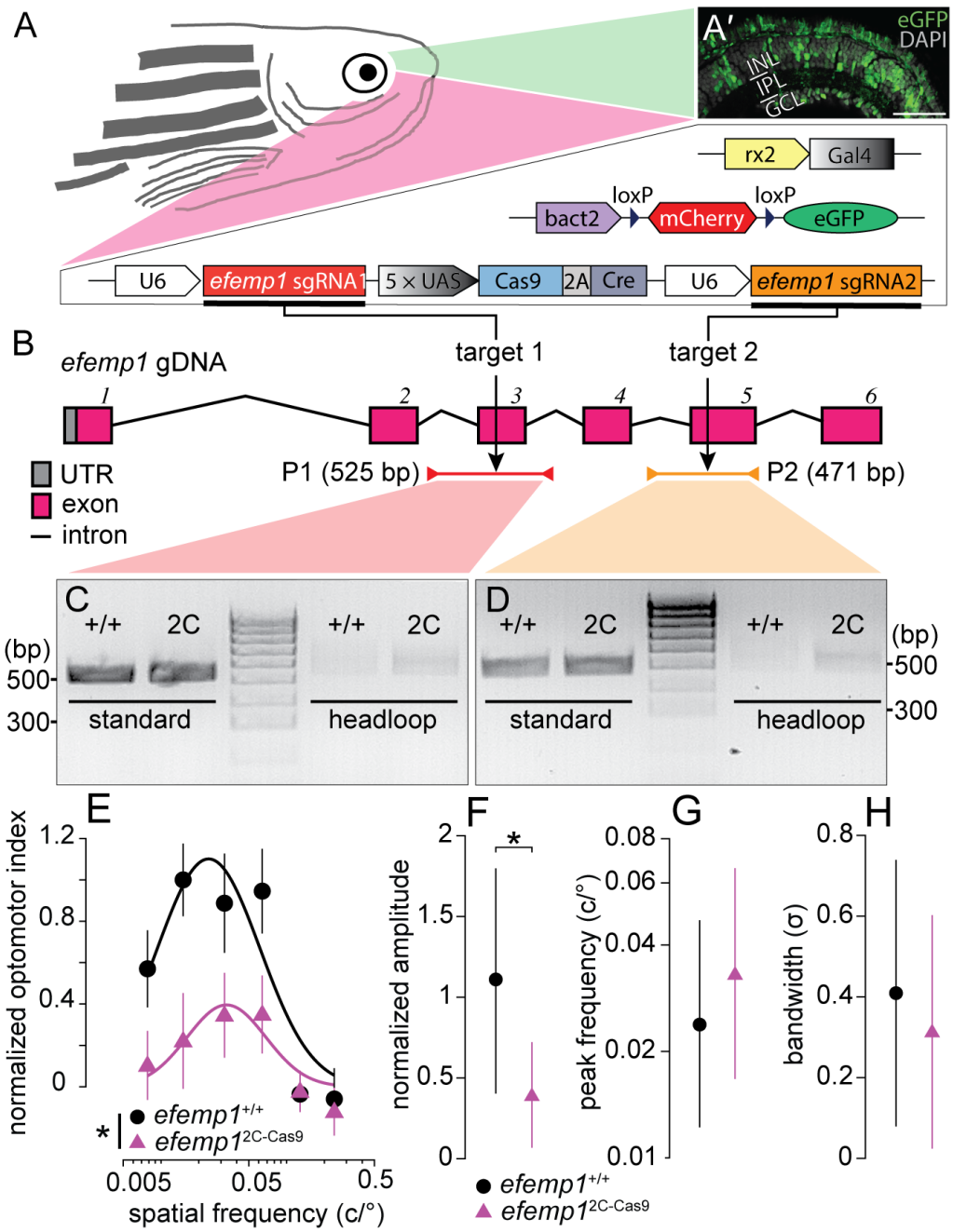

Figure 1. **Genotypic details of retina-specific *efemp1*-knockout 2C-Cas9 mutants (*efemp1*$^{2C\text{-}Cas9}$) and phenotypic verification via optomotor responses at 5 days post-fertilization (dpf). (A)** The *efemp1*$^{2C\text{-}Cas9}$ fish were generated using 2C-Cas9 somatic gene editing. Mutant fish have three separate transgenes: Tg(*rx2*:*Gal4*) × Tg(*bact2-loxP-mCherry-loxP-eGFP*) × Tg(*UAS*:*Cas9T2ACre*;*U6*:*efemp1sgRNA1*;*U6*:*efemp1sgRNA2*). Co-expression of these transgenic elements result in expression of green fluorescence (eGFP) in zebrafish retina, indicative of successful Cas9 protein expression. **(A′)** Representative retinal image from a 6 dpf fish. Nuclei stained with DAPI are shown in grey. INL, inner nuclear layer; IPL, inner plexiform layer; GCL, ganglion cell layer. Scale bar: 40 µm. **(B)** The universally expressed *efemp1* sgRNA1 and sgRNA2 from the transgene binds with Cas9 nucleases and cuts exons 3 and 5 of the *efemp1* genome DNA (gDNA), respectively. Standard PCR primers used for genotyping the target sites 1 and 2 amplified 525- (Product 1, P1; spinning from the introns before to after the exon 3) and 471-base pairs (bp; P2; spinning from the intron before to the end of exon 5) of DNA sequences, respectively. Products of headloop PCR are 23-bp longer for P1 and 20-bp longer for P2 due to the headloop tags in reverse primers. UTR, untranslated region. **(C–D)** Gel electrophoresis of the products from standard and headloop PCR for genotyping targeted sites 1 **(C)** and 2 **(D)**. In both images, the middle lanes show a 100-bp reference ladder; positions of 300 and 500 bp of size are indicated for both gel images. **(E–H)** Results of optomotor responses. Spatial-frequency tuning functions **(E)** for 5 dpf *efemp1*$^{+/+}$ (n = 14) and *efemp1*$^{2C\text{-}Cas9}$ fish (n = 13) are three-parameter log-Gaussian functions fit to the data by minimizing the least-square error. The fitted parameters, including **(F)** normalized amplitude, **(G)** peak frequency and **(H)** bandwidth, were compared between groups **Group data are shown** as mean ± SEM in (E) and mean with 95% confidence intervals in (F–H). *$P < 0.05$ (*F*-test).

134 **Disruption of *efemp1* causes myopia and abnormal ocular development in zebrafish**

135 We investigated the development of ocular refraction in *efemp1*$^{2C\text{-}Cas9}$ mutant zebrafish using optical
136 coherence tomography (OCT) to non-invasively obtain cross-section images of zebrafish eyes. This
137 allowed us to quantify ocular refraction as the ratio of retinal radius to lens radius (R/L ratio; Fig 2A),
138 namely *Matthiessen's Ratio*, which is a common means to return axial ocular refraction for aquatic
139 species (Collery et al., 2014; Shand et al., 1999; Turnbull et al., 2015). A higher R/L ratio compared to
140 control fish indicates relative axial myopia, while a lower ratio represents a relative hyperopic shift.
141 Overall, *efemp1*$^{2C\text{-}Cas9}$ fish have higher R/L ratio than *efemp1*$^{+/+}$ fish ($P = 0.0002$), indicating relative
142 myopic ocular structure. *Post-hoc* analysis identified significant relative axial myopia at 2, 6 and 8
143 weeks of age ($P = 0.018$, 0.0001 and 0.002, respectively; Fig 2B).

144 We considered why axial myopia was not significant at 4 wpf in *efemp1*$^{2C\text{-}Cas9}$ fish. EGFP fluorescence
145 levels in the eye appeared to vary between *efemp1*$^{2C\text{-}Cas9}$ fish. We speculated that *efemp1*$^{2C\text{-}Cas9}$ fish with
146 higher eGFP expression indicating higher Cas9 nuclease expression and thus higher rate of CRISPR
147 gene editing, would have more severe visual impairment. As visual impairment can impact feeding, we
148 examined survival rate in low (eGFP+) and high eGFP (eGFP+++) expressing *efemp1*$^{2C\text{-}Cas9}$ fish,
149 differences that were easily distinguished via *post-hoc* histology (Fig 2C). Those *efemp1*$^{2C\text{-}Cas9}$ fish with
150 weaker retinal eGFP expression had higher survival rates than GFP+++ group ($P < 0.0001$; Fig 2C).
151 About 10% of GFP+ fish were lost by 2 wpf ($P = 0.020$) but survival was stable thereafter. In contrast,
152 GFP+++ fish had significantly lower survival rates than GFP+ group at 2 and 4 wpf ($P = 0.0007$ and P
153 < 0.0001, respectively). The survival rate stabilized in GFP+++ from 4 wpf. We interpret these data to
154 indicate that at 4 wpf, loss of the more myopic fish may have contributed to the absence of a significant
155 effect at this age (Fig 2C).

156 We also found that at 5–8 months of age, 7.11% of *efemp1*$^{2C\text{-}Cas9}$ fish appear to have monocular or
157 binocular enlargement (154 fish in total from 5 tanks; Table S1; Fig 2F–I, yellow arrows), compared to
158 *efemp1*$^{+/+}$ fish (Fig 1D–E). In some cases, there was a dark crescent between the eye socket and the
159 ventral eyeball (Fig 2H, white dashed area). Dissection of this eye showed aggressive posterior eye
160 expansion and a scleral crack (Fig 2H insert). Further study is required to confirm whether these rare,

161 severe scleral cracks represented a greater or faster ocular expansion caused by our retinal *efemp1*

162 modification. Overall, the above results suggest that disruption of *efemp1*$^{2C\text{-}Cas9}$ leads to myopic vision,

163 eye enlargement, and possibly more severe ocular pathology.

164

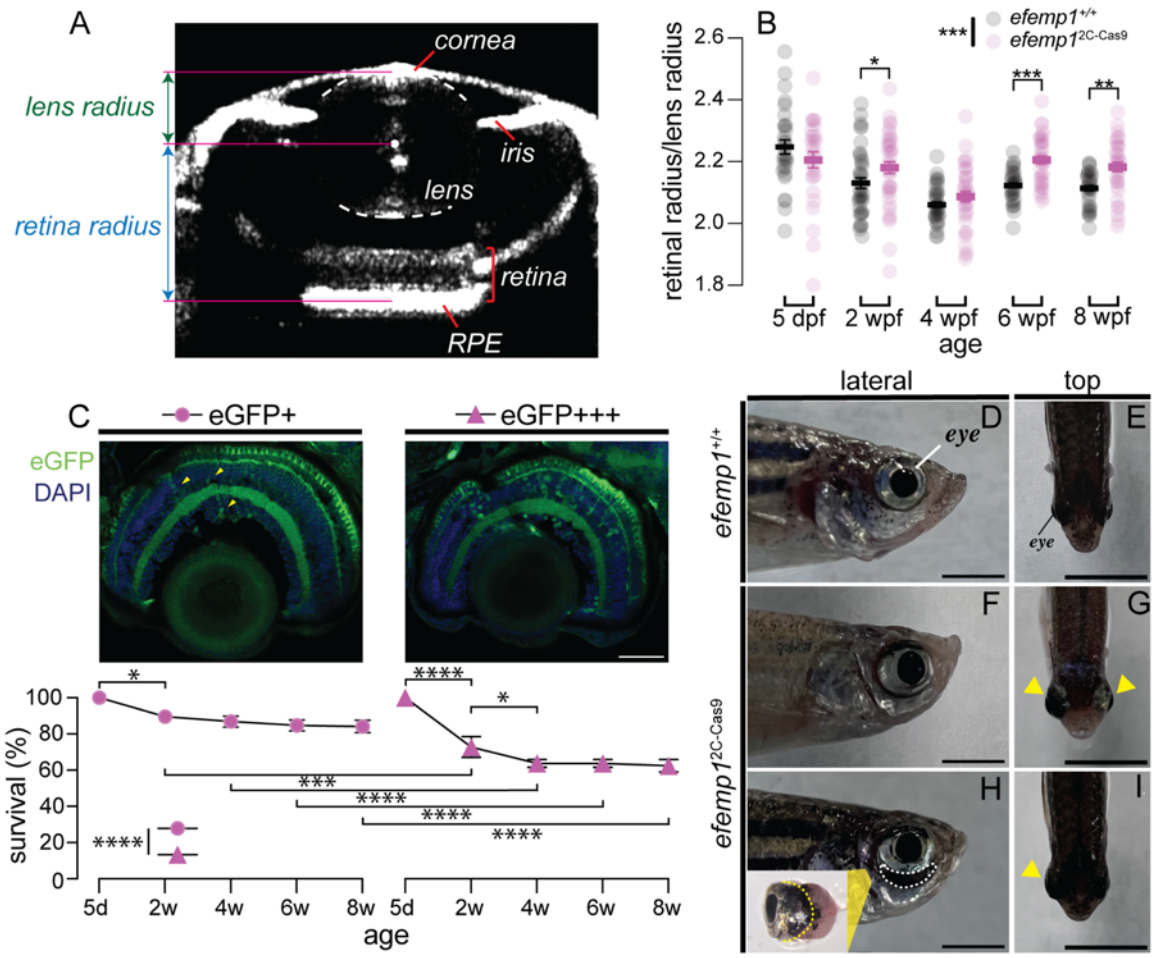

165

166 Figure 2. **Ocular development of *efemp1*$^{2C\text{-}Cas9}$ fish under normal rearing.** (A) Representative optical coherence tomography
167 (OCT) image showing eye components, including the cornea, iris, lens, retina and retinal pigment epithelium (RPE). Relative
168 ocular refraction was calculated as the ratio of retinal radius to lens radius. **(B)** Ocular refraction of *efemp1*$^{+/+}$ and *efemp1*$^{2C\text{-}Cas9}$
169 fish at 5 days post-fertilization (dpf; n = 30 and 29 eyes, respectively), and 2 (n = 40 per genotype), 4 (n = 40 and 38 eyes,
170 respectively), 6 (n = 39 and 40 eyes, respectively), and 8 weeks post-fertilizations (wpf; n = 40 and 34 eyes, respectively)**. (C)**
171 *Efemp1*$^{2C\text{-}Cas9}$ fish were categorized into two groups based on their retinal eGFP levels (eGFP+ vs. eGFP+++). Sporadic eGFP
172 positive cells (highlighted by yellow arrows) are evident in the eGFP+ retinal image, whereas the eGFP+++ retinal image had
173 more EGFP cells. Scale bar: 40 µm. Survival rates for eGFP+ and eGFP+++ groups from 5 days (d; set as 100%) to 8 weeks (w)
174 of age are presented as mean ± SEM. Three tanks per group were analyzed. *$P < 0.05$; **$P < 0.01$; ****$P < 0.0001$. *Two*-way
175 ANOVA and Fisher's LSD *post-hoc* tests were performed. In **(C)**, for comparisons within each eGFP level, only significant survival
176 differences between a time point and its adjacent time are shown. **(D–I)** Representative images of eye morphology for
177 *efemp1*$^{+/+}$ **(D–E)** and *efemp1*$^{2C\text{-}Cas9}$ fish **(F–I)** reared under normal lighting at 1 year old. Yellow arrowheads indicate enlarged
178 eyes. Dashed region below the eye in **(H)** highlights a scleral crack shown in the zoom-in image insert, in which the yellow
179 dashed line indicates the estimated normal position of the posterior eye of zebrafish. Scale bars: 3 mm.

180 **EFEMP1 deficits in the retina results in altered retinal function**

181 The retina plays a crucial role in the local regulation of eye growth, a process that does not require input
182 from the brain (Troilo et al., 1987; Wallman et al., 1987). To examine whether retinal function is
183 involved in the abnormal development of ocular refraction in the *efemp1*$^{2C\text{-}Cas9}$ fish, electroretinograms
184 (ERG) were recorded at 2, 4, 6 and 8 wpf.

185 At 2 weeks of age, *efemp1*$^{2C\text{-}Cas9}$ fish showed significantly lower photoreceptoral *a*-wave amplitude (P
186 $= 0.0118$), especially at higher stimulus intensities (Fig 3A$_2$), compared to *efemp1*$^{+/+}$ fish. However, *b*-
187 wave amplitude was similar between mutants and control fish (Fig 3A$_1$). *A*- and *b*-wave implicit times
188 of *efemp1*$^{2C\text{-}Cas9}$ fish were significantly faster than that of *efemp1*$^{+/+}$ fish ($P = 0.018$ and 0.0047,
189 respectively; Fig 3A, 4A$_3$–A$_4$).

190 At 4 wpf (Fig 3B–B$_4$), *efemp1*$^{2C\text{-}Cas9}$ fish showed smaller *b*-wave amplitude ($P < 0.0001$; Fig 3B$_1$), but
191 no difference in *a*-wave amplitude (Fig 3B$_2$) compared with *efemp1*$^{+/+}$ fish. *Two*-way ANOVA also
192 indicated significantly slower *b*-wave ($P = 0.0052$, Fig 3B$_3$) and *a*-wave ($P < 0.0001$, Fig 3B$_4$) in
193 *efemp1*$^{2C\text{-}Cas9}$ fish.

194 At 6 wpf, both *a*- and *b*-wave amplitudes were significantly smaller in *efemp1*$^{2C\text{-}Cas9}$ relative to *efemp1*$^{+/+}$
195 fish (effects of genotypes: $P < 0.0001$ for both *a*- and *b*-wave; Fig 3C–C$_2$). *Efemp1*$^{2C\text{-}Cas9}$ fish had
196 significantly slower *b*-wave (effect of genotypes: $P = 0.0182$, Fig 3C$_3$) and *a*-wave responses ($P =$
197 0.0068 for –2.11 log cd.s.m^{-2}; Fig 3C$_4$) than *efemp1*$^{+/+}$ fish.

198 At 8 wpf (Fig 3D), both *b*-wave ($P = 0.012$; Fig 3D$_1$) and *a*-wave amplitudes ($P < 0.0001$; Fig 3D$_2$)
199 were a little larger in *efemp1*$^{2C\text{-}Cas9}$ compared to *efemp1*$^{+/+}$ fish. A clear effect of genotypes was evident
200 in terms of slower *b*-waves ($P = 0.0012$; Fig 3D$_3$) and *a*-waves ($P = 0.015$; Fig 3D$_4$) in *efemp1*$^{2C\text{-}Cas9}$
201 fish. A longer latency before initiation of the *b*-wave might expose a larger proportion of the electro-
202 negative photoreceptoral *a-wave* responses, accounting for the observed larger but slower *a-waves*.

203 Although it is unclear why *efemp1*$^{2C\text{-}Cas9}$ mutants show faster response at a young age, but slower
204 response at 4-8 wpf, it is apparent that retinal dysfunction is a robust phenotype of this genetic myopia
205 mutant model.

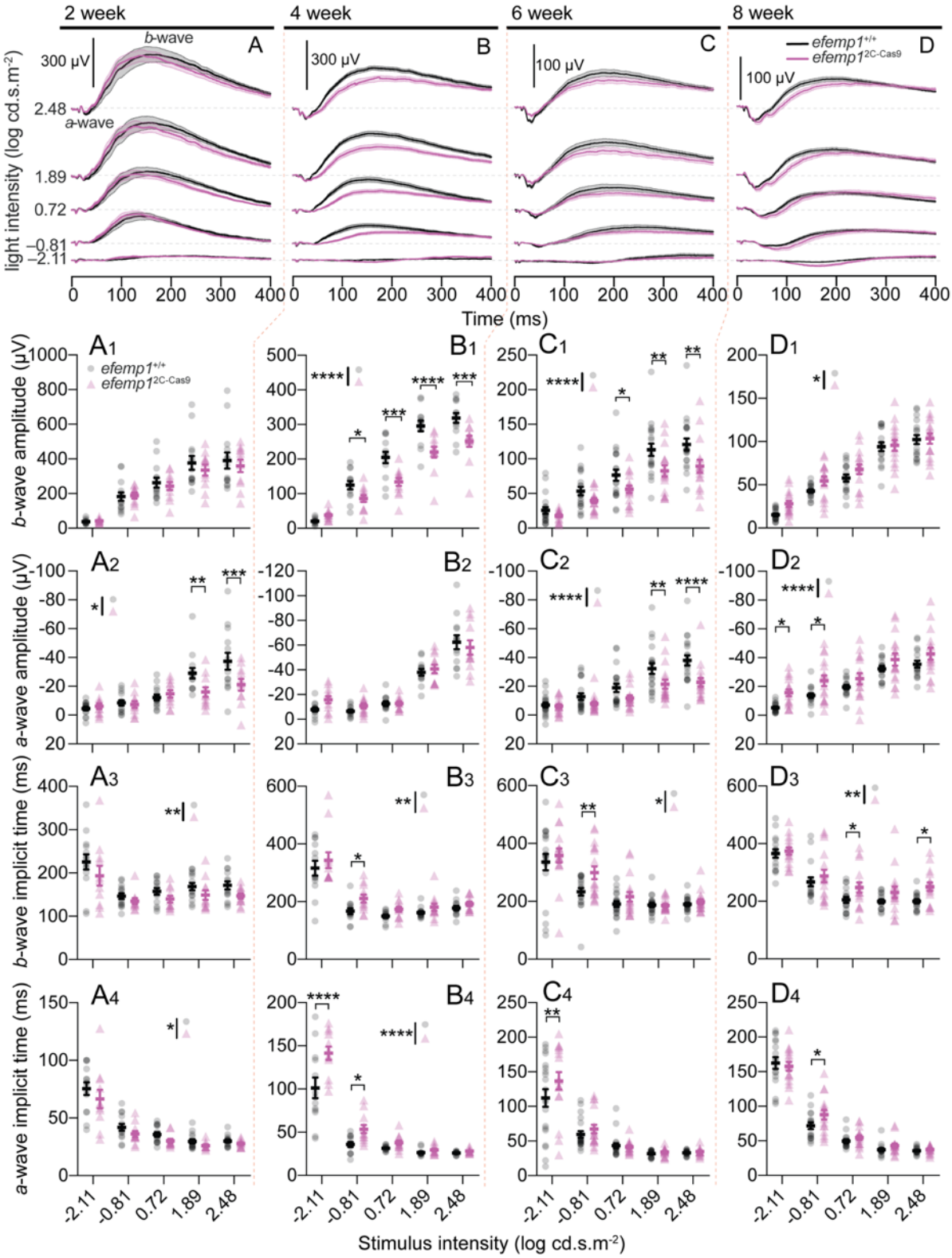

Figure 3. **Electroretinogram (ERG) results of *efemp1*$^{+/+}$ and *efemp1*$^{2C\text{-}Cas9}$ fish under normal rearing. (A, B, C, D)** Group average ERG traces with shades areas indicating SEM, **(A_1, B_1, C_1, D_1)** *b*-wave amplitudes, **(A_2, B_2, C_2, D_2)** *a*-wave amplitudes, **(A_3, B_3, C_3, D_3)** *b*-wave implicit times and **(A_4, B_4, C_4, D_4)** *a*-wave implicit times at 2 **(A–A_4, respectively)**, 4 **(B–B_4, respectively)**, 6 **(C–C_4, respectively)** and 8 **(D–D_4, respectively)** weeks post-fertilization (wpf). There were 14 and 11 eyes for 2 wpf, 13 and 12 eyes for 4 wpf, 20 and 17 eyes for 6 wpf, and 17 and 16 eyes for 8 wpf *efemp1*$^{+/+}$ and *efemp1*$^{2C\text{-}Cas9}$ fish, respectively. Scale bars: 300 µV in **(A–B)** and 100 µV in **(C–D)**. Group data are shown as mean ± SEM. *T*wo-way ANOVA and Fisher's LSD *post-hoc* tests were performed. **P < 0.05*; ***P< 0.01*; ****P < 0.001*; *****P < 0.0001*.

214 **Zebrafish with retinal *efemp1* disruption become emmetropic after dark-rearing**

215 As our results showed that *efemp1* disruption led to myopia development in zebrafish under normal
216 lighting, we further investigated whether *efemp1* modification might exacerbate the myopia-inducing
217 effects of dark-rearing (Fig 4A) (Xie et al., 2023 Preprint).

218 After 2 weeks of rearing under normal lighting, *efemp1*$^{2C\text{-}Cas9}$ fish had developed myopia compared with
219 *efemp1*$^{+/+}$ fish ($P < 0.0001$). Interestingly, after 2 weeks of dark-rearing, *efemp1*$^{2C\text{-}Cas9}$ fish did not
220 undergo a myopic shift ($P < 0.0001$, Fig 4B), and had similar ocular fraction to *efemp1*$^{+/+}$ fish reared
221 under normal light.

222 After 4 weeks of dark-rearing, control *efemp1*$^{+/+}$ fish became myopic ($P = 0.025$; Fig 4B). However,
223 similar to 2-week results, relative to normal-light-reared *efemp1*$^{+/+}$ fish, *efemp1*$^{2C\text{-}Cas9}$ fish were myopic
224 when reared under normal lighting ($P < 0.0001$), but after dark-rearing they maintained a R/L ratio that
225 was consistent with emmetropic vision at this age (Fig 4B).

226 A *three*-way ANOVA reveals a significant interaction between genotypes and environmental conditions
227 ($P < 0.0001$). These results indicated that under normal visual conditions *efemp1* is needed for
228 emmetropization, however under aberrant visual conditions the lack of *efemp1* can interfere with
229 mechanisms that usually drive myopia development.

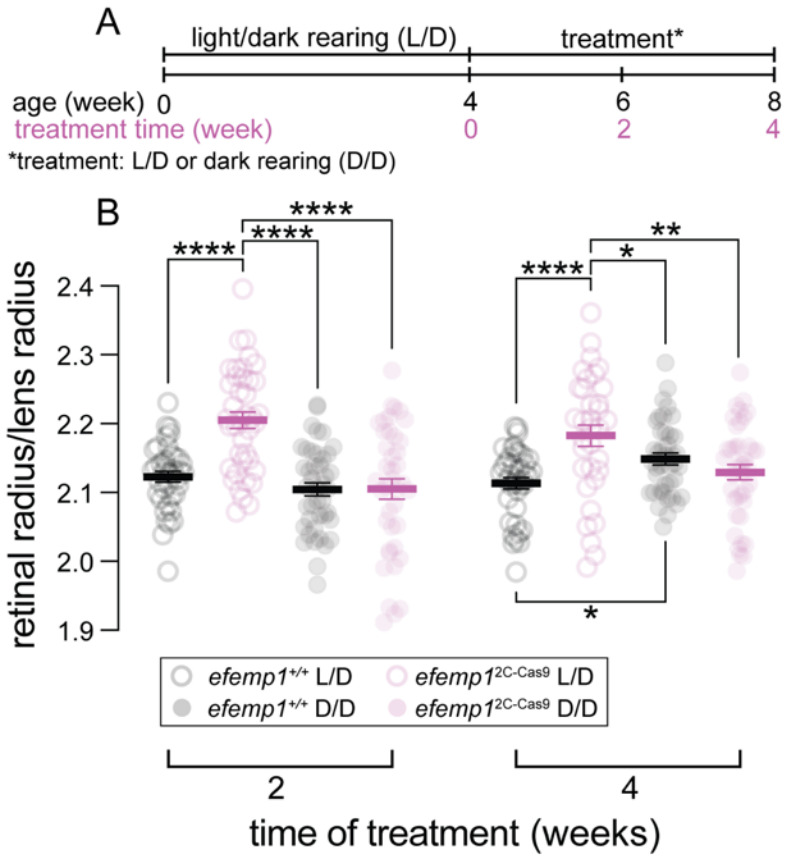

Figure 4. **Ocular refraction of *efemp1*$^{+/+}$ and *efemp1*$^{2C\text{-}Cas9}$ fish after environmental treatment. (A)** *Efemp1*$^{+/+}$ and *efemp1*$^{2C\text{-}Cas9}$ fish were reared under normal light/dark cycle (L/D) until 4 weeks post-fertilization (wpf) and either continued under normal lighting (L/D) or switched to dark-rearing (D/D) for 2 or 4 weeks (to 6 or 8 wpf, respectively). **(B)** Relative ocular refraction of L/D- or D/D-reared *efemp1*$^{+/+}$ and *efemp1*$^{2C\text{-}Cas9}$ eyes were quantified after 2 or 4 weeks of treatment using optical coherence tomography (OCT). There were 39, 40, 42 and 40 eyes at the 2-week time point, and 40, 34, 40 and 40 eyes at the 4-week time point for L/D-reared *efemp1*$^{+/+}$, L/D-reared *efemp1*$^{2C\text{-}Cas9}$, D/D-reared *efemp1*$^{+/+}$, D/D-reared *efemp1*$^{2C\text{-}Cas9}$ fish, respectively. Group data are shown as mean ± SEM. *Three*-way ANOVA and Fisher's LSD *post-hoc* analyses were performed. *$P < 0.05$; **$P < 0.01$; ***$P < 0.001$; ****$P < 0.0001$.

Retinal *efemp1* modification drives retinal physiological changes in response to dark-rearing

To investigate whether *efemp1* is involved in dark-rearing-induced retinal functional changes, we analyzed ERG of *efemp1*$^{+/+}$ and *efemp1*$^{2C\text{-}Cas9}$ fish after 2 days, 2 or 4 weeks of normal light or dark-rearing.

After 2 days of treatment, under either rearing condition, *efemp1*$^{2C\text{-}Cas9}$ fish showed smaller ERG responses than *efemp1*$^{+/+}$ fish (Fig 5A–D). *Three*-way ANOVA confirmed a significant genotype effect with smaller *b*- and *a*-wave amplitudes, as well as slowed *b*- and *a*-wave implicit times ($P < 0.0001$, $P = 0.0002$, $P = 0.0023$ and $P = 0.021$, respectively; Fig 5E–H) for *efemp1*$^{2C\text{-}Cas9}$ fish. There was a

248 significant interaction between genotypes and rearing conditions for *b*-wave implicit time (*P = 0.0362*;
249 Fig 5G).

250 Functional outcomes after 2-weeks treatment (Fig 5I–L) were similar to those for 2 days of treatment.
251 In general *b*- and *a*-wave amplitudes (*P < 0.0001* for both; Fig 5M–N) were smaller in *efemp1*$^{2C\text{-}Cas9}$
252 fish. After dark-rearing, *efemp1*$^{2C\text{-}Cas9}$, but not *efemp1*$^{+/+}$ fish showed further *b*-wave reduction (*P =*
253 *0.031* at 1.87 log cd.s.m^{-2}; Fig 5M). *Three*-way ANOVA returned significant interactions between
254 genotype and dark-rearing on *a*-wave amplitude (*P = 0.0396*), with *efemp1* disruption further
255 attenuating dark-rearing-induced photoreceptor responses (Fig 5N). In particular, after dark-rearing, *a*-
256 wave amplitudes were smaller at all tested intensities for *efemp1*$^{+/+}$ fish (*P = 0.042*, *P = 0.0004* and *P <*
257 *0.0001* for –0.83, 0.73 and 1.87 log cd.s.m^{-2}, respectively), but only at the highest intensity for *efemp1*$^{2C\text{-}}$
258 ^{Cas9} fish (*P = 0.0009*; Fig 5N). We did not find difference in *b*-wave implicit time between groups (Fig
259 5O), however both *efemp1*$^{+/+}$ and *efemp1*$^{2C\text{-}Cas9}$ fish had slower *a*-wave implicit time after dark-rearing
260 at –0.83 log cd.s.m^{-2} (*P = 0.012* and *0.010*, respectively; Fig 5P). Overall, these results suggested that
261 *efemp1* modification exacerbates functional changes seen with dark-rearing.

262 At the 4-week time point, under either rearing condition *efemp1*$^{2C\text{-}Cas9}$ fish had smaller and slower *b*-
263 waves than *efemp1*$^{+/+}$ fish (*P < 0.0001* and *P = 0.002*, respectively; Fig 5Q–T, 5U and 5W,). *A*-waves
264 in mutants were slightly larger and slower (Fig 5V and 5X, *P < 0.0001*). The waveform indicates that
265 slower *b*-waves expose more of the photoreceptoral response, making the *a*-wave both larger and slower.

266 Taken together, at 2 dpf and 2 wpf, significant statistical interactions indicate that *efemp1* modification
267 affects the way that dark-rearing impacts retinal physiology.

268

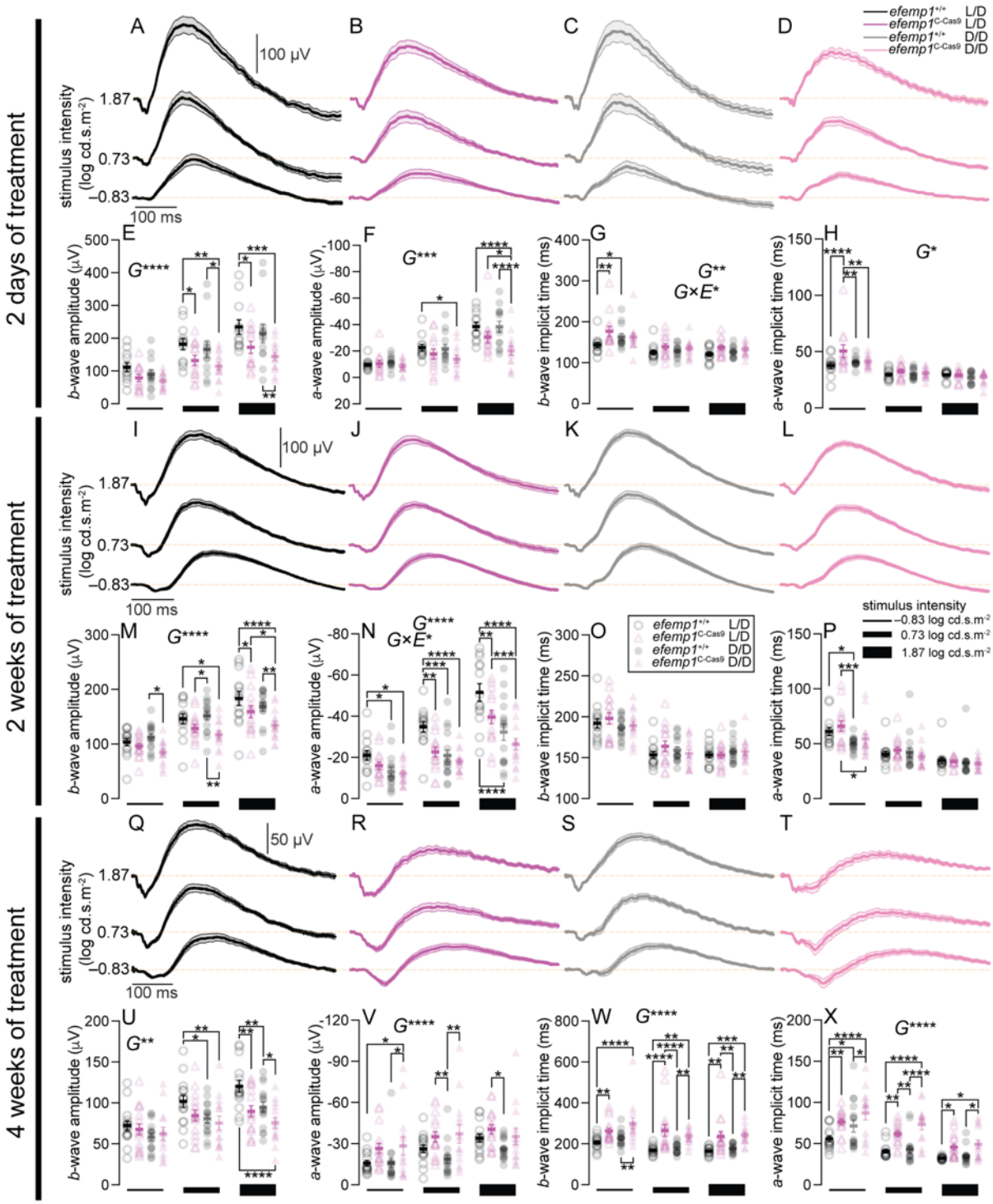

Figure 5. **Electroretinography (ERG) of *efemp1*$^{+/+}$ and *efemp1*$^{2C\text{-}Cas9}$ fish after 2 days, 2 weeks or 4 weeks of light/dark-cycle (L/D) or dark (D/D) rearing.** (A–H) Group average ERG traces for **(A)** L/D-reared *efemp1*$^{+/+}$ (n = 12), **(B)** L/D-reared *efemp1*$^{2C\text{-}Cas9}$ (n = 13), **(C)** D/D-reared *efemp1*$^{+/+}$ (n = 13) and **(D)** D/D-reared *efemp1*$^{2C\text{-}Cas9}$ eyes (n = 14). Shaded areas indicated SEM. Group **(E)** *b*-wave amplitude, **(F)** *a*-wave amplitude, **(G)** *b*-wave implicit time and **(H)** *a*-wave implicit times measured after 2 days of treatment. Vertical scale bar indicates 100 µV and horizontal scale bar represents 100 ms in **(A–D)**. **(I–P)** Group average ERG traces for **(I)** L/D-reared *efemp1*$^{+/+}$ (n = 14), **(J)** L/D-reared *efemp1*$^{2C\text{-}Cas9}$ (n = 15), **(K)** D/D-reared *efemp1*$^{+/+}$ (n = 16) and **(L)** D/D-reared *efemp1*$^{2C\text{-}Cas9}$ eyes (n = 15), as well as their **(M)** *b*-wave amplitude, **(N)** *a*-wave amplitude, **(O)** *b*-wave implicit time and **(P)** *a*-wave implicit time measured after 2 weeks of treatment. **(Q–X)** Group average ERG traces for **(Q)** L/D-reared *efemp1*$^{+/+}$ (n = 15), **(R)** L/D-reared *efemp1*$^{2C\text{-}Cas9}$ (n = 16), **(S)** D/D-reared *efemp1*$^{+/+}$ (n = 16) and **(T)** D/D-reared *efemp1*$^{2C\text{-}Cas9}$ eyes (n = 14), as well as their **(U)** *b*-wave amplitude, **(V)** *a*-wave amplitude, **(W)** *b*-wave implicit time and **(X)** *a*-wave implicit time measured after 4 weeks of treatment. Group data are shown as mean ±SEM. ERGs were measured at –0.83, 0.73 and 1.87 log cd.s.m^{-2} of stimulus intensities, represented by black blocks of different sizes below

graphs; thicker blocks indicate higher intensities. *Three*-way ANOVA and Fisher's LSD *post-hoc* tests were performed. Significant main effects of genotypes (*G*) and interactions between genotypes and rearing conditions (*G*×*E*) are indicated in the graphs. *$P < 0.05$; **$P < 0.01$; ***$P < 0.001$; ****$P < 0.0001$.

Retinal *efemp1* modification changes expression of myopia-associated genes under normal rearing and their responses to dark-rearing

In order to investigate potential molecular pathways through which retinal *efemp1* modification impacts refractive development under normal and dark-rearing, we quantified expression of a group of known myopia-associated genes using RT-qPCR after 2 days and 4 weeks of environmental manipulation. These timepoints broadly align with initiation (2 days) and consolidation (4 weeks) phases of myopia development in zebrafish (Fig 6A).

We first quantified the expression of *efemp1,* and found lower *efemp1* expression in *efemp1*$^{2C\text{-}Cas9}$ than in *efemp1*$^{+/+}$ fish under normal and dark-rearing ($P = 0.0248$ and 0.0295, respectively) but only at the later time point (Fig 6B).

The *early growth response 1* (*egr1*) gene is an immediate early response transcriptional factor that has been shown to be up-regulated when the eye is exposed to hyperopia-inducing or myopia-suppressing visual environments, and down-regulated when the eye is under myopia-inducing visual conditions (Ashby et al., 2014; Fischer et al., 1999). Loss of this gene promots myopia in mice (Schippert et al., 2007). In our data, there were genotype ($P = 0.042$) and dark-rearing effects ($P < 0.0001$) on *egr1* expression. After 2 days of normal light rearing, *egr1* expression was up-regulated in *efemp1*$^{2C\text{-}Cas9}$ fish compared to *efemp1*$^{+/+}$ fish (~ 4 wpf; $P = 0.0002$). *Egr1* expression was then down-regulated later after 4 weeks in normal lighting (8 wpf; $P = 0.018$). After 2 days of dark-rearing, both genotypes showed reduced *egr1* expression ($P < 0.0001$ for both). After 4 weeks of dark-rearing, only *efemp1*$^{+/+}$ fish showed down-regulated *egr1* expression ($P = 0.0011$) and no further change was seen in *efemp1*$^{2C\text{-}Cas9}$ fish (Fig 6C).

Transforming growth factor beta genes (*tgfbs)* encode fundamental secreted TGF-βs, which has been shown to be down-regulated in form-deprived myopic tree shrew eyes to impact collagen synthesis (Jobling et al., 2004) and in particular matrix metalloproteinase 2 (MMP2) (Itoh et al., 2010). Our results

310 showed that expression of *tgfb1a* was impacted by genotype and rearing condition (*P = 0.0292* and
311 *0.0070*, respectively). At the 4-week timepoint, under either normal or dark-rearing, *efemp1*$^{2C\text{-}Cas9}$ fish
312 showed lower *tgfb1a* expression than *efemp1*$^{+/+}$ fish (*P = 0.0038* and *0.0205*, respectively). *Tgfb1a*
313 expression was reduced in both *efemp1*$^{+/+}$ and *efemp1*$^{2C\text{-}Cas9}$ fish after dark-rearing (*P = 0.0051* and
314 *0.0271*, respectively; Fig 6D). The expression of *tgfb1b* was primarily influenced by dark-rearing (*P =*
315 *0.0047*); both *efemp1*$^{+/+}$ and *efemp1*$^{2C\text{-}Cas9}$ fish showed a reduction after 4 weeks of dark-rearing (*P =*
316 *0.0003* and *0.0041*, respectively; Fig 6E).

317 The *vascular endothelial growth factor A* (*vegfa*) gene encodes the glycoprotein VEGFA, which
318 contributes to vasculature development, neuronal function (Mackenzie and Ruhrberg, 2012) and
319 extracellular matrix regulation (Kuiper et al., 2007). Decreased retinal VEGFA concentration was found
320 in marmosets with lens-induced myopia (Zhu et al., 2021). For the two zebrafish *vegfa* paralogues,
321 *three*-way ANOVA showed an effect of dark-rearing on expression of both *vegfaa* and *vegfab* (*P <*
322 *0.0001* for both). Both *efemp1*$^{+/+}$ and *efemp1*$^{2C\text{-}Cas9}$ fish showed decreased *vegfaa* expression after 2 days
323 (*P = 0.0094* and *0.0026*, respectively) and 4 weeks of dark-rearing (*P = 0.0002* and *0.012*, respectively;
324 Fig 6F). *Vegfab* down-regulation was found in both *efemp1*$^{+/+}$ and *efemp1*$^{2C\text{-}Cas9}$ fish after 2 days of dark-
325 rearing (*P < 0.0001* and *P = 0.0007*, respectively) but was only observed in *efemp1*$^{+/+}$ fish at week 4 (*P*
326 *= 0.0001*). A significant interaction between genotypes and rearing conditions shown by *three*-way
327 ANOVA analysis (*P = 0.0125*), is indicative of a smaller dark-rearing-induced reduction in *vegfab*
328 expression due to *efemp1* disruption. Indeed, retinal *efemp1* disruption *per se* had led to a down-
329 regulation of *vegfab* under normal rearing (*P = 0.039* and *0.035* at the 2-day and 4-week time points,
330 respectively; Fig 6G).

331 Insulin-like growth factor 1 (IGF1), an endocrine growth hormone, is produced in the liver and then
332 delivered to other organs, playing an important role in overall growth during development
333 (Stratikopoulos et al., 2008). A previous study reported that *igf1* was up-regulated in form-deprived
334 myopic guinea pigs (Ding et al., 2020). However, we did not observed difference in *igf1* expression
335 between groups in our experiments (Fig 6H).

336 Fibroblast growth factor (FGF2) has functions in embryonic development, angiogenesis, wound healing,
337 cell differentiation and neuronal function (e.g., photoreceptor transduction) (Bikfalvi et al., 1997). With
338 form-deprivation myopia, *fgf2* expression was reported to be down-regulated in the chick sclera but up-
339 regulated in guinea pig retinae (An et al., 2012; Seko et al., 1995). Our *three*-way ANOVA analysis
340 showed an effect of rearing conditions on *fgf2* expression ($P = 0.0432$). Only *efemp1*$^{+/+}$ but not *efemp1*$^{2C-}$
341 ^{Cas9} fish showed a reduction of *fgf2* expression after 2 days of dark-rearing ($P = 0.0392$), suggesting that
342 *efemp1* disruption may attenuate dark-rearing induced changes in *fgf2* expression (Fig 6I). Yet, our data
343 showed no statistical significance for a gene-environment interaction.

344 The *Wnt family 2B* (*wnt2b*) gene activates the Wnt/β-catenin signaling pathway which is crucial for
345 ocular development (e.g., lens, retinal pigment epithelium, vasculature and rod photoreceptors, etc.)
346 (Blomfield et al., 2023). Mice with form-deprivation myopia were found to show up-regulated *wnt2b*
347 expression (Ma et al., 2014). Our statistics showed a significant interaction between genotype and
348 rearing condition ($P = 0.0096$; Fig 6J). *Efemp1*$^{+/+}$ fish, but not *efemp1*$^{2C\text{-}Cas9}$ fish, showed down-
349 regulation of *wnt2b* expression after 2 days of dark-rearing ($P = 0.0003$), implicating reduced dark-
350 rearing-induced changes in *wnt2b* expression with *efemp1* deficiency.

351 The soluble retinol binding protein 3 (RBP3; or IRBP in mammals) is released into the
352 interphotoreceptor matrix from retinal photoreceptors, mediating retinoid trafficking for the visual cycle
353 (Gonzalez-Fernandez and Ghosh, 2008). Lack of *Rbp3* in mice caused excessive eye growth and myopia
354 (Wisard et al., 2011). In both *efemp1*$^{+/+}$ and *efemp1*$^{2C\text{-}Cas9}$ fish, *rbp3* expression was down-regulated after
355 2 days ($P = 0.0007$ and $P < 0.0001$, respectively) and 4 weeks of dark-rearing ($P < 0.0001$ for both; Fig
356 6K). Rearing condition thus made a major effect on expression of *rbp3* ($P < 0.0001$). Retinal *efemp1*
357 modification also resulted in significantly higher *rbp3* expression in *efemp1*$^{2C\text{-}Cas9}$ fish ($P = 0.044$),
358 particularly after 2 days under normal rearing ($P = 0.0144$; Fig 6K).

359 The *gap junction delta 2* (*gjd2*) gene encodes a predominant gap junction protein, connexin36, in the
360 central nervous system, including the retina, forming electrical synapses for rapid neuronal signaling
361 (Bloomfield and Völgyi, 2009). Recent findings showed that depletion of the two zebrafish paralogues,

362 *gjd2a* and *gjd2b*, caused myopia and hyperopia, respectively (Quint et al., 2021). We found no
363 expression changes in *gjd2a* expression between groups (Fig 6L). In contrast, *three*-way ANOVA
364 analysis showed a main effect of rearing conditions on *gjd2b* expression ($P < 0.0001$). Both *efemp1*$^{+/+}$
365 and *efemp1*$^{2C\text{-}Cas9}$ fish showed an up-regulation after 2 days ($P = 0.0261$ and 0.0368, respectively) and
366 4 weeks of dark-rearing ($P < 0.0001$ and $P = 0.0003$, respectively; Fig 6M).

367

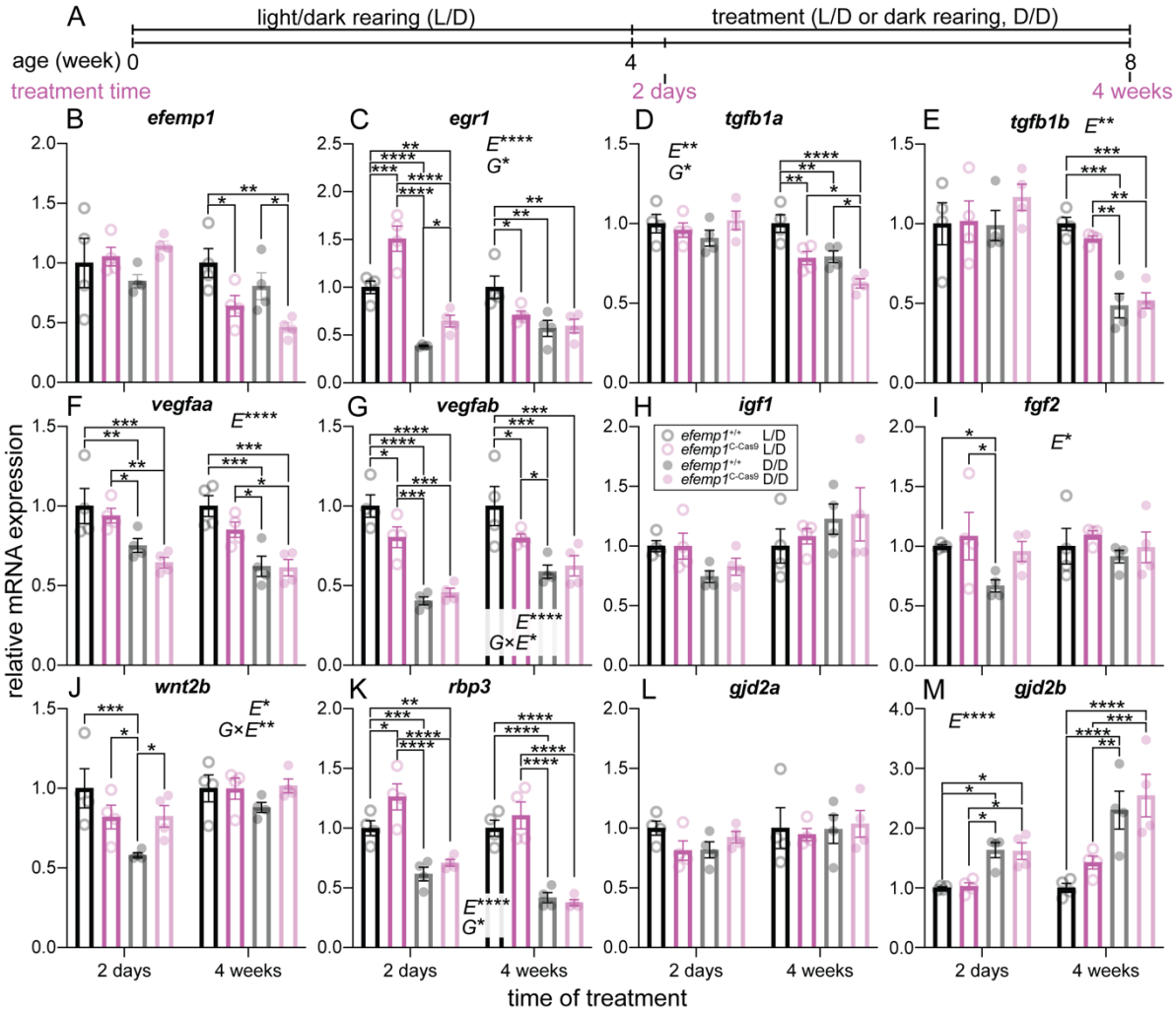

368

369 Figure 6. **Expression of representative myopia-associated genes for *efemp1*$^{+/+}$ and *efemp1*$^{2C\text{-}Cas9}$ fish after 2 days or 4 weeks**
370 **of light/dark-cycle (L/D) or dark (D/D) rearing. (A)** *Efemp1*$^{+/+}$ and *efemp1*$^{2C\text{-}Cas9}$ fish were reared under a standard light/dark-
371 cycle (L/D) to 4 weeks post-fertilization (wpf) and then were reared under L/D or dark tanks (D/D) to up to 8 wpf (4 weeks of
372 treatment). Eyes for molecular analysis were sampled after 2 days or 4 weeks of treatment. Relative mRNA levels of myopia-
373 associated genes, including **(B)** *efemp1*, **(C)** *egr1*, **(D)** *tgfb1a*, **(E)** *tgfb1b*, **(F)** *vegfaa*, **(G)** *vegfab*, **(H)** *igf1*, **(I)** *fgf2*, **(J)** *wnt2b*, **(K)**
374 *rbp3*, **(L)** *gjd2a*, **(M)** *gjd2b* were analyzed for *efemp1*$^{+/+}$ and *efemp1*$^{2C\text{-}Cas9}$ fish after 2 days and 4 weeks of treatment (n = 4
375 samples per group), using qPCR. Group data are shown as mean ± SEM. *Three*-way ANOVA and Fisher's LSD *post-hoc* tests
376 were performed. Significant main effects of genotypes (*G*), rearing conditions (*E*) and their interactions (*G*×*E*) are indicated in
377 the graphs. *$P < 0.05$; **$P < 0.01$; ***$P < 0.001$; ****$P < 0.0001$.

378

379 **Differences in EFEMP1, TIMP2 and MMP2 distributions between *efemp1*$^{+/+}$ and *efemp1*$^{2C\text{-}Cas9}$ fish**
380 **were found after normal and dark-rearing**

381 We examined whether retinal *efemp1* modification affects the distribution of myopia-associated
382 extracellular matrix proteins in the retina after 2 days or 4 weeks of normal or dark-rearing (Fig 7A).

383 With the mosaic pattern of retinal *efemp1* modification (Fig 2C), EFEMP1 protein expression was still
384 evident in the retina (Fig 7B–C). We found that at the 2-day timepoint, *efemp1*$^{2C\text{-}Cas9}$ fish showed a
385 change in EFEMP1 distribution with relatively lower levels in the amacrine cell layer (ACL; effect of
386 genotypes: $P = 0.0079$; Fig 7B$_{1–4}$ and 7B$_{i–ii}$) but higher relative expression in the inner plexiform layer
387 (IPL) compared with *efemp1*$^{+/+}$ fish ($P = 0.0132$; Fig 7B$_{1–2}$ and B$_{i–iii}$). After 2 days of dark-rearing, inner
388 retinal EFEMP1 distribution remained largely unchanged in both genotypes (Fig 7B). At the 4-week
389 timepoint, dark-rearing reduced EFEMP1 expression in the ACL in both genotypes (effect of rearing
390 conditions: $P < 0.0001$; Fig 7C$_{1–4}$ and 7C$_{i–ii}$). A significant interaction was observed for the ganglion
391 cell layer (GCL; $P = 0.0022$; Fig 7C$_{i}$ and C$_{iv}$), with *efemp1*$^{2C\text{-}Cas9}$ fish ($P = 0.0015$), but not *efemp1*$^{+/+}$
392 fish, exhibiting higher relative EFEMP1 expression in the GCL after dark-rearing.

393 Matrix metalloproteinase 2 (MMP2) and tissue inhibitor of metalloproteinase 2 (TIMP2) have long
394 been associated with myopia (Jia et al., 2017; Jia et al., 2014; Liu and Sun, 2018) and our previous data
395 showing that their distribution was changed after dark-rearing (Xie et al., 2023 Preprint).

396 Analyzing their inner retinal distribution, we found that at the 2-day timepoint, relative TIMP2
397 expression in *efemp1*$^{2C\text{-}Cas9}$ fish was overall lower in the ACL but higher in the IPL, compared to control
398 *efemp1*$^{+/+}$ fish (effect of genotypes: $P = 0.0001$ and $P < 0.0001$, respectively; Fig 7D$_{1–4}$ and 7D$_{i–iii}$).
399 Dark-rearing reduced relative TIMP2 expression in the GCL for *efemp1*$^{+/+}$ ($P = 0.0015$) but not
400 *efemp1*$^{2C\text{-}Cas9}$ fish, showing a gene-environment interaction ($P = 0.0069$; Fig 7D$_{i}$ and 7D$_{iv}$). At the 4-
401 week timepoint, overall dark-rearing reduced relative TIMP2 expression in the ACL and GCL (effect
402 of rearing conditions: $P = 0.0067$ and 0.0021, respectively; Fig 7E$_{1–4}$, 7E$_{i–ii}$ and 7E$_{iv}$). In the IPL, after
403 dark-rearing, relative TIMP2 expression seemed to be reduced in *efemp1*$^{2C\text{-}Cas9}$ fish but slightly
404 increased in *efemp1*$^{+/+}$ fish, exhibiting a gene-environment interaction ($P = 0.025$; Fig 7E$_{iii}$).

For MMP2, in the ACL, 2 days of dark-rearing overall resulted in higher MMP2 expression (effect of environment: $P = 0.0008$) in *efemp1*$^{+/+}$ fish but not in *efemp1*$^{2C\text{-}Cas9}$ fish (gene-environment interactions: $P = 0.0079$; Fig 7F$_{1–4}$ and 7F$_{i–ii}$). In the GCL, after 2 days of normal rearing, *efemp1*$^{+/+}$ fish had higher relative MMP2 expression than *efemp1*$^{2C\text{-}Cas9}$ fish ($P = 0.0064$; Fig 7F$_{1–2}$ and 7F$_{i–iv}$). 2 days of dark-rearing overall led to increased MMP2 expression in the GCL (effect of rearing conditions: $P < 0.0001$); this increase was greater in *efemp1*$^{2C\text{-}Cas9}$ than in *efemp1*$^{+/+}$ fish (effect of gene-environment interactions: $P < 0.0075$; Fig 7F$_{1–4}$, 7F$_{i}$ and 7F$_{iv}$). At the 4-week timepoint, MMP2 expression pattern was affected by dark-rearing, with lower relative expression in the ACL but higher expression in the IPL and GCL (effect of environment: $P < 0.0001$, $P = 0.0002$ and $P < 0.0001$, respectively; Fig 7G).

Overall, inner retinal distributions of EFEMP1, TIMP2 and MMP2 can be affected by either *efemp1* disruption or dark-rearing. More importantly, retinal *efemp1* modification impacts, in a time dependent manner, how dark-rearing-affects the redistribution of inner retinal proteins.

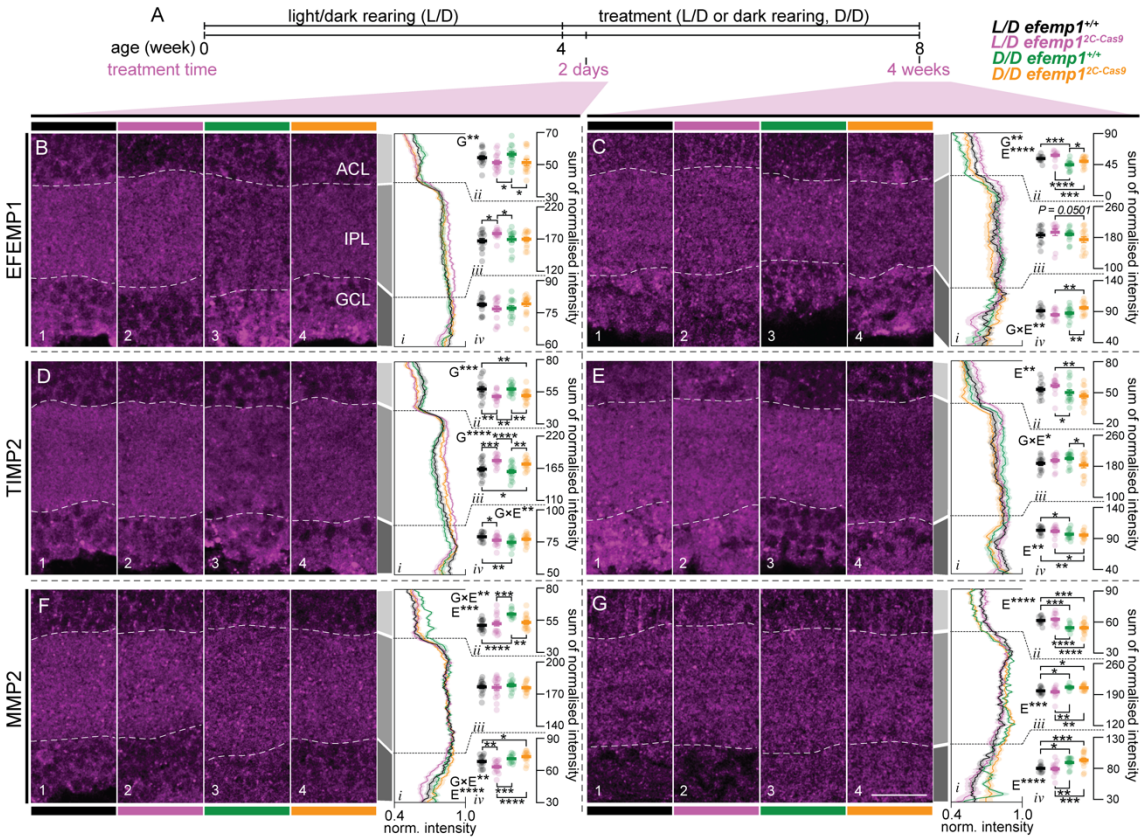

Figure 7. **Distribution of EFEMP1, TIMP2 and MMP2 in the inner retina of *efemp1*$^{+/+}$ and *efemp1*$^{2C\text{-}Cas9}$ fish after 2 days or 4 weeks of normal light/dark (L/D) cycle or dark (D/D) rearing. (A)** *Efemp1*$^{+/+}$ and *efemp1*$^{2C\text{-}Cas9}$ fish were reared under standard L/D condition to 4 weeks post-fertilization (wpf) and then were under L/D- or D/D-rearing to up to 8 wpf (4 weeks of treatment). Eyes for histological analysis were sampled after 2 days or 4 weeks of treatment. **(B–C)** Immunostaining for EFEMP1 to analyze its distribution in the inner retina, including amacrine cell layer (ACL), inner plexiform layer (IPL) and ganglion cell layer (GCL),

for L/D-reared *efemp1*$^{+/+}$, L/D-reared *efemp1*$^{2C\text{-}Cas9}$, D/D-reared *efemp1*$^{+/+}$ and D/D-reared *efemp1*$^{2C\text{-}Cas9}$ fish after 2 days (**B**; n = 16, 16, 14 and 14 retinae, respectively) and 4 weeks (**C**; n = 12, 12, 15 and 14 retinae, respectively) of treatment. White dash lines in micrographs highlight the borders of the IPL. Average normalized expression across the inner retina is shown in **(B*i* and C*i*)** and summed normalized expression (normalized intensity) for **(B*ii* and C*ii*)** ACL, **(B*iii* and C*iii*)** IPL and **(B*iv* and C*iv*)** GCL was quantified for each eye. **(D–E)** Immunostaining for TIMP2 in the inner retina for L/D-reared *efemp1*$^{+/+}$, L/D-reared *efemp1*$^{2C\text{-}Cas9}$, D/D-reared *efemp1*$^{+/+}$ and D/D-reared *efemp1*$^{2C\text{-}Cas9}$ fish after 2 days (**D**; n = 16, 16, 16 and 15 retinae, respectively) and 4 weeks (**E**; n = 13, 14, 15 and 14 retinae, respectively) of treatment. Average normalized expression is shown in **(D*i* and E*i*)** and summed normalized expression for **(D*ii* and E*ii*)** ACL, **(D*iii* and E*iii*)** IPL and **(D*iv* and E*iv*)** GCL. **(F–G)** Immunostaining for MMP2 for L/D-reared *efemp1*$^{+/+}$, L/D-reared *efemp1*$^{2C\text{-}Cas9}$, D/D-reared *efemp1*$^{+/+}$ and D/D-reared *efemp1*$^{2C\text{-}Cas9}$ fish after 2 days (**F**; n = 16, 16, 12 and 15 retinae, respectively) and 4 weeks (**G**; n = 13, 13, 12 and 15 retinae, respectively) of treatment. Average normalized expression is shown in **(F*i* and G*i*)** and summed normalized expression for **(F*ii* and G*ii*)** ACL, **(F*iii* and G*iii*)** IPL and **(F*iv* and G*iv*)** GCL . Scale bar in **(G)** represents 20 µm and all images share the same scale. Group data are shown as mean ± SEM. *Two*-way ANOVA and Fisher's LSD *post-hoc* tests were performed. Significant main effects of genotypes (*G*), rearing conditions (*E*) and their interactions (*G*×*E*) are indicated in the graphs. **P < 0.05*; ***P < 0.01*; ****P < 0.001*; *****P < 0.0001*.

Discussion

In this study, we showed that retina-specific *efemp1* down-regulation leads to enlarged eyes and myopia development in zebrafish (Fig 2B, 2D–I). This resembles the progressive myopia that has been reported in human patients with loss-of-function *efemp1* mutations (Driver et al., 2020). However, mice with *efemp1* knockout showed no alternations in gross ocular structure, retinal function nor visual acuity, but did show progressive corneal maldevelopment (Daniel et al., 2020). Unfortunately, the authors did not analyze ocular refraction in their loss-of-function mouse model. In addition to aberrant eye growth, our mutants had reduced spatial visual sensitivity (Fig 1E–H, Fig S1) and altered retinal function (Figs 3 and 5). Particularly striking was the progressive slowing of the ERG in *efemp1*$^{2C\text{-}Cas9}$ fish with older ages (Fig 3 and 5). This resembles the age-related slowing of *b*-wave implicit time reported in some, but not all, human patients with Malattia Leventinese, a retinal dystrophy caused by a gain-of-function *efemp1* mutation (c.1033C>T, p.Arg345Trp) (Gerber et al., 2003). Taken together, *efemp1* mutant zebrafish show phenotype characteristics indicative of both gain- and loss-of-function mutations.

Concurrence of gain- and loss- of function *efemp1* mutations in our mutants could be expected; with the 2C-Cas9 system, CRISPR gene editing independently occurred in retinal neurons expressing the Cas9 nuclease, leading to different types of indels even within an individual retina. Despite these mutations being mosaic and perhaps of low efficiency (Fig 1C–D) in our model, the phenotype was robust, indicating that tight control of finely balanced *efemp1* expression is required for optimal ocular development. However, this does demonstrate the importance of using the 2C-Cas9 system with caution for studies requiring specific gain or loss of function mutations. Our data showed a down-regulation of

458 *efemp1* in *efemp1*$^{2C\text{-}Cas9}$ fish at 8 weeks of age (Fig 6B). In contrast, a recent study reported increased
459 EFEMP1 in tears sampled from myopic human patients and increased EFEMP1 in myopic guinea pig
460 choroid (Shi et al., 2023). To understand these species related differences, tissue specific comparative
461 studies would be required.

462 For our ERG results, although slower ERG responses were a robust phenotype in *efemp1*$^{2C\text{-}Cas9}$ fish at
463 the older ages, at 2 wpf *a*- and *b*-wave implicit times were actually faster than control *efemp1*$^{+/+}$ fish
464 (Fig 3A_3–A_4). One possible explanation is that *efemp1*$^{2C\text{-}Cas9}$ fish had shorter axial length than *efemp1*$^{+/+}$
465 fish at this age ($P < 0.0001$, unpaired *t*-test; Fig S2) and thus effectively higher retinal illumination.

466 We noticed that under normal rearing, *efemp1*$^{2C\text{-}Cas9}$ fish had larger *a*-wave amplitudes at 8 wpf (or 4-
467 week timepoint in the dark-rearing experiment) than *efemp1*$^{+/+}$ fish, which we attributed to slower *b*-
468 wave onset exposing more of the *a*-wave (Fig 3D_2 and Fig 5V). *B-wave* effects in 8 wpf *efemp1*$^{2C\text{-}Cas9}$
469 fish were less consistent, with slightly higher *b*-wave amplitudes in one experiment (Fig 3D_1) but
470 smaller *b*-waves in another (Fig 5U). We speculated that this might arise from variability in gene editing
471 (as discussed above) between retinae (and batches), leading to different severities and phenotypes.
472 Nonetheless, it is clear that *efemp1* function causes retinal dysfunction in zebrafish.

473 Under dark-rearing, retinal dysfunction in *efemp1*$^{2C\text{-}Cas9}$ was exacerbated (Fig 5), but this did not lead to
474 worsening myopia (Fig 4). One speculation is that without visual input (dark-rearing) in the presence
475 of *efemp1* disruption the zebrafish eye shuts down light-dependent signals for ocular growth and
476 switches to intrinsic mechanisms for ocular growth regulation, thus leading to emmetropic vision. This
477 idea requires investigation.

478 Our survival analysis suggested that *efemp1*$^{2C\text{-}Cas9}$ mutants at 4 wpf did not show a myopic shift. This
479 could be due to a number of factors. Firstly, because those fish with a higher level of visual impairment
480 and perhaps early-onset myopia are those likely to have been lost by 4 wpf. Thus, those fish with lower
481 mutation rates and better vision were more likely survived to older ages allowing more time (>4 weeks)
482 for the development of myopia (Fig 2C). Secondly, changes in *egr1* expression shown in our data (Fig
483 6C) may also be a separate contributor to the observed absent myopic shift in 4 wpf *efemp1*$^{2C\text{-}Cas9}$ fish.
484 Previous studies suggest that *egr1* may have a role in signaling bi-directional ocular growth (Ashby et

485 al., 2014; Fischer et al., 1999). Up-regulated *egr1* expression in 2-day normal-light-reared (~4 wpf)
486 *efemp1*$^{2C\text{-}Cas9}$ fish showed evidence myopia suppression, whereas down-regulation of *egr1* in 4-week
487 normal-light-reared (equivalent to 8 wpf) *efemp1*$^{2C\text{-}Cas9}$ fish showed a myopic shift (Fig 6C). The
488 direction of these expression changes qualitatively matched ocular refraction of *efemp1*$^{2C\text{-}Cas9}$ fish at the
489 corresponding ages (Fig 2B).

490 In our gene expression data, down-regulation of *tgfb1a* and *vegfab* was associated with myopia
491 development in *efemp1*$^{2C\text{-}Cas9}$ fish under normal lighting (Fig 6E and 6G) (Jobling et al., 2004; Zhu et
492 al., 2021). Dark-rearing-induced down-regulation of *egr1*, *tgfb1s*, *vegfaa*, *fgf2* and *rbp3*, and up-
493 regulation of *gjd2b* were not impacted by *efemp1* modification (Fig 6C, 6D–F, 6I, 6K and 6M), with
494 two exceptions being *vegfab* and *wnt2b* (Fig 6G and 6J). Despite the similarities in dark-rearing-induced
495 gene expression, *efemp1*$^{+/+}$ fish became myopic after 4 weeks of dark-rearing, *efemp1*$^{2C\text{-}Cas9}$ fish
496 remained emmetropic (Fig 4). It is possible that *efemp1* functional integrity is required to manifest
497 dark-rearing-induced phenotypes with changes in these genes. We speculate that without normal *efemp1*
498 expression under dark-rearing, intrinsic mechanisms may take over and regulate ocular growth. Future
499 investigations are required to verify this hypothesis.

500 The genes *wnt2b* (Fig 6J) and *vegfab* (Fig 6 G), were down-regulated only in *efemp1*$^{+/+}$ but not *efemp1*$^{2C\text{-}}$
501 ^{Cas9} fish after 2 days and 4 weeks of dark-rearing, respectively, suggesting that dark-rearing requires
502 normal *efemp1* expression to induce and maintain their expression changes, respectively. EFEMP1 has
503 been previously shown to suppress the epithelial-mesenchymal transition in endometrial carcinoma
504 through Wnt/β-catenin signaling, for which WNT2B is an activator (Blomfield et al., 2023; Yang et al.,
505 2016). Further investigation might target interactions between EFEMP1, WNT2B and EMT in myopia
506 development. Importantly, the impact of *efemp1* modification on dark-rearing-induced *vegfab*
507 expression further implies a light-dependent signaling between *efemp1* and *vegfab* than is crucial for
508 ocular growth.

509 There was up-regulation of *rbp3* expression in normal-light-reared *efemp1*$^{2C\text{-}Cas9}$ fish at the 2-day but
510 not at the 4-week timepoint (Fig 6K). It is likely that *efemp1* deficiency altered the interphotoreceptor
511 matrix and thus impairing the visual cycle and *11-cis* retinal supply (Gonzalez-Fernandez and Ghosh,

512 2008; Yue, 2014). Up-regulating *rbp3* may be a compensatory response in young zebrafish. Myopia
513 development has been reported in *gjd2b* knockout zebrafish (Quint et al., 2021), however our data
514 showed robust *gjd2* up-regulation in both phenotypes under myopia-inducing dark-rearing (Fig 6M).
515 Whether this up-regulation reflect feedback remains to be clarified.

516 In our histological analysis, distribution changes of EFEMP1 in the inner retina under different rearing
517 conditions indicate retinal *efemp1* modification at the post-transcriptional level (Fig 7B–C). In addition,
518 our data indicated that *efemp1* modification affects the way that inner retinal MMP2 (particularly after
519 2 days) and TIMP2 (particularly after 4 weeks) were impacted in response to dark-rearing (Fig 7D–G).
520 There have been previous reported that changes in expression of EFEMP1 in cultured endothelial cells
521 led to decreased MMP2 but unchanged TIMP2 expression (Albig et al., 2006), highlighting a context-
522 dependent regulation of EFEMP1. In future studies, it will be worth analyzing other MMPs (e.g., MMP3,
523 etc.) and TIMPs (e.g., TIMP1 and TIMP3, etc.) that have been associated with EFEMP1 (Livingstone
524 et al., 2020) and eye elongation (Jia et al., 2017; Jia et al., 2014).

525 In summary, the modification of retinal *efemp1* in zebrafish resulted in reduced spatial visual sensitivity,
526 axial myopia, eye enlargement, altered retinal function, myopia-associated gene expression changes
527 (i.e., *egr1*, *efemp1*, *tgfb1a*, *vegfab*, *rbp3*), and redistribution of inner retinal EFEMP1, TIMP2 and
528 MMP2 proteins, under normal rearing. Under dark-rearing, *efemp1*$^{2C\text{-}Cas9}$ fish did not develop myopia,
529 even though dark-rearing seemed to worsen retinal function. We found *efemp1*-dependent responses of
530 *vegfab* and *wnt2b* expression to dark-rearing, highlighting signaling between *efemp1* and these genes
531 as likely mechanisms involved in visually regulated ocular development. Dark-rearing-induced
532 redistribution of EFEMP1, TIMP2 and MMP2 were also influenced by *efemp1* disruption. This study
533 provides robust evidence that *efemp1* regulates ocular development and visual function in a light-
534 dependent manner, with several potential myopia-associated molecular pathways implicated for further
535 investigation. We illustrated a valuable zebrafish analysis platform combining environmental and
536 genetic manipulations, as well as multifaced analyses for high-throughput investigation of the growing
537 number of myopia-risk genes to gain insight into their interactions with visual environment in myopia
538 development.

539 ## Materials and Methods

540 ### Animal husbandry

541 All procedures were performed according to the provisions of the Australian National Health and
542 Medical Research Council code of practice for the care and use of animals and were approved by the
543 Faculty of Science Animal Ethics Committee at the University of Melbourne (Project No. 10399).

544 For standard husbandry, zebrafish (Danio rerio; transgenic fish, see detailed description below) were
545 maintained and bred in the Fish Facility at the University of Melbourne according to local animal
546 guidelines. Embryos and larvae (prior to sex determination) were grown in Petri dishes in an incubator
547 at 28.5°C up to 5 days post-fertilization (dpf), then introduced to tanks under normal 14h/10h light/dark
548 (L/D) cycles and raised in flow-through systems at 28°C.

549 For dark (D/D) rearing, zebrafish tanks were wrapped using black cloth tapes (Model number
550 66623336603; Bear brand, Saint-Gobain Abrasives, Somerton, VIC, Australia) to block light. Zebrafish
551 were induced to blackout tanks at 4 wpf and reared in darkness for 2 days, 2 or 4 weeks. Age-matched
552 fish reared under standard lighting were used as environmental control. Zebrafish health condition and
553 survival were monitored daily using dim red light (LED; 17.4 $cd.m^{-2}$, λ_{max} 600 nm).

554

555 ### Generation of mutants

556 In this study, we used a novel somatic CRISPR gene editing system, namely 2C-Cas9 (Di Donato et al.,
557 2016), to generate the retina-specific knockout mutant of the *efemp1* gene. The
558 p*UAS*:*Cas9T2ACre*;*U6*:*sgRNA1*;*U6*:*sgRNA2* plasmid (Addgene #74010) was digested using BsaI
559 (R0535S; NEB, Ipswich, MA, USA) and BsmBI-v2 enzymes (R0739S; NEB) targeting the restriction
560 sites behind the U6 promoters to remove the pre-set sequences that are to be replaced by DNA sequences
561 of small guide RNA (sgRNA). Digested vectors were purified using a QIAquick Gel Extraction kit
562 (28704; Qiagene, Hilden, Germany). Double-strand DNAs of the two sgRNAs (oligos shown in Table
563 S2), *efemp1sgRNA1* and *efemp1sgRNA2*, were annealed from single-strand oligos and inserted into the
564 digested vector using T4 DNA ligase (M0467S; NEB). Ligated plasmids were transformed into α-select
565 chemically competent cells (BIO-85026; Bioline, London, UK). Positively transformed cells were

566 selected using antibiotic Ampicillin LB agar plates and colonies were picked to grow in Ampicillin LB
567 medium at 37°C for overnight. Plasmids were extracted and purified using a QIAprep Spin Miniprep
568 kit (27106; Qiagene). Successful insertions of DNAs into the plasmid were determined by sequence-
569 specific PCR, gel electrophoresis and Sanger sequence (Fig S3B). Concentrations of extracted plasmids
570 were quantified using a Nanodrop 1000 (Thermo Fisher Scientific; Waltham, MA, USA). *Efemp1*
571 sgRNAs targeting exons were designed based on the *efemp1* genome DNA sequence (gDNA;
572 ENSDARG00000059121) using the *CHOPCHOP* online tool (Labun et al., 2019) and pre-tested *in*
573 *vitro* using a GenCrispr sgRNA Screening kit (Fig S3A;L00689; GenScript, NJ, USA) before insertion
574 into vectors. The two sgRNAs target exons 3 and 5 of *efemp1* gDNA. Tol2 transposase mRNA was
575 transcribed from a p*tol2* plasmid (kind gift from Dr. Mirana Ramialison, Murdoch Children's Research
576 Institute) using a mMESSAGE mMACHINE SP6 Transcription Kit (AM1340; Thermo Fisher
577 Scientific).

578 To generate the retina-specific *efemp1* modification in zebrafish, we co-injected
579 p*UAS*:*Cas9T2ACre*;*U6*:*efemp1sgRNA1*;*U6*:*efemp1sgRNA2* at a concentration of 35 ng/µl and *tol2*
580 mRNA at 50 ng/µl into embryos of fish Tg(*bact2-loxP-mCherry-loxP-eGFP*) × Tg(*rx2*:*Gal4*).
581 Expression of the injected plasmid were identified based on green fluorescence (eGFP) in the zebrafish
582 eyes observed under a fluorescence microscope at 3 dpf. F0 fish with green fluorescent eyes were mated
583 with transgenic fish Tg(*bact2-loxP-mCherry-loxP-eGFP*) × Tg(*rx2*:*Gal4*) to screen for the founders
584 that had the 2C-Cas9 transgene integrated into the germ line. In this study, we used transgenic fish
585 Tg(*bact2-loxP-mCherry-loxP-eGFP*) × Tg(*rx2*:*Gal4*), namely *efemp1*$^{+/+}$ fish as the control of the
586 mutant fish Tg(*bact2-loxP-mCherry-loxP-eGFP*) × Tg(*rx2*:*Gal4*) ×
587 Tg(*UAS*:*Cas9T2ACre*;*U6:efemp1sgRNA1*;*U6:efemp1sgRNA2*), named *efemp1*$^{2C\text{-}Cas9}$ fish. These fish
588 also have a transgene Tg(*UAS*:*nfsb-mCherry*) that was driven by the retina-specific Tg(*rx2*:*Gal4*),
589 leading to much brighter red fluorescence signals in the zebrafish eye than in the body, where *mCherry*
590 expression was triggered by Tg(*bact2-loxP-mCherry-loxP-eGFP*). These allowed to sort Tg(*rx2*:*Gal4*)
591 positive fish for *efemp1*$^{+/+}$ fish. *Efemp1*$^{2C\text{-}Cas9}$ fish were sorted by eye-specific green fluorescence, which
592 indicated presence of Tg(*rx2*:*Gal4*), without the need to the Tg(*UAS*:*nfsb-mCherry*) reporter. However,

593 to ensure that the only genetic difference between *efemp1*$^{+/+}$ and *efemp1*$^{2C\text{-}Cas9}$ fish was from the 2C-
594 Cas9 construct Tg(*UAS*:*Cas9T2ACre*;*U6:efemp1sgRNA1*;*U6:efemp1sgRNA2*), we also used fish with
595 bright red eyes indicating existence of Tg(*UAS*:*nfsb-mCherry*) for mutant groups. As the Tg(*UAS*:*nfsb-*
596 *mCherry*) was not directly relevant to the 2C-Cas9 gene editing system and our phenotypic assessments,
597 for a simplified demonstration, we did not highlight this transgene construct in this report.

598 For genotyping, we used a headloop PCR protocol (Kroll et al., 2021). Standard PCR Primers were
599 designed using Primer Premier 5.0 (Singh et al., 1998) and headloop PCR primers were designed using
600 a published Python script (Kroll et al., 2021) (see Table S3 for oligo information). GDNA was isolated
601 from 7 dpf *efemp1*$^{+/+}$ or *efemp1*$^{2C\text{-}Cas9}$ zebrafish eyes using a Monarch Genomic DNA Purification Kit
602 (T3010S; NEB) and quantified using a Nanodrop 1000 (Thermo Fisher Scientific). In a PCR reaction,
603 there were 30 ng gDNA of either genotype, 0.25 µl 10 mM forward primer, 0.25 µl 10 mM reverse
604 primer, 5 µl Hot Start High-Fidelity 2× Master Mix (M0494S; NEB) and nuclease-free water to fill up
605 to 10 µl. The PCR program was comprised of an initial denaturation step of 98°C for 30 seconds, 32
606 cycles of 98°C for 15 seconds, 60°C for 15 seconds, and 72°C for 15 seconds, followed by a final
607 extension step of 72°C for 2 minutes. Electrophoresis of the PCR products was performed using 2%
608 Tris-acetate-EDTA (TAE) agarose gel.

609

610 **Optomotor response (OMR)**

611 The OMR apparatus was adapted from that previously described (Xie et al., 2019a; Xie et al., 2021;
612 Xie et al., 2019b). A Power Mac G5 computer (Apple Computer, Inc., Cupertino, CA, USA) ran
613 MATLAB 2016b (MathWorks, Natick, MA, USA) with Psychtoolbox extensions (Kleiner et al., 2007).
614 Stimuli were processed on an ATI Radeon HD 5770 graphics card, with the output sent to a BITS++
615 video processor (Cambridge Research Systems, Rochester, UK) for increased contrast resolution for
616 stimuli displayed on a M992 flat-screen cathode ray tube (CRT) monitor (Dell Computer Corporation,
617 Round Rock, TX, USA) with its screen facing upwards. During experiments, a zebrafish was placed in
618 a custom annulus swimming chamber (the inner and outer walls were 29.5 and 46.5 mm from the center,
619 respectively) with a transparent base positioned 46 mm above the screen. A C922 Pro Stream webcam

620 (Logitech Company, Lausanne, Switzerland; 1080p at 30 Hz), placed 130 mm above the swimming
621 chamber base, controlled using MATLAB recorded videos of each trial for *post-hoc* analysis of
622 zebrafish angular movement.

623 During a trial, a test stimulus was displayed on the CRT screen below the swimming chamber, rotating
624 at 0.5 rad/s for 30s. Test stimuli were windmill sinusoidal gratings with central spatial frequencies of
625 0.0078, 0.0155, 0.0310, 0.0620, 0.1240 and 0.2480 cycle per degree (c/°). A blank grey screen was
626 presented between test stimuli. Test stimuli were generated using the green and blue channels of the
627 CRT monitor with constant red luminance across the screen. A long pass filter (cut-off wavelength
628 600nm) was fixed to the front of a camera to filter out blue and green light, allowing only red light to
629 pass through, thus eliminating the moving stimulus and allowing better visualization of the fish for
630 analysis.

631 OMR was measured for 5 dpf and 2 wpf *efemp1*$^{+/+}$ and *efemp1*$^{2C\text{-}Cas9}$ zebrafish, after acclimating fish to
632 the swimming chamber for 5 minutes. All experiments were conducted between 9:00 AM and 7:00 PM.
633 After experiments, fish were humanely killed using 1000 ppm AQUIS (#106036, Primo Aquaculture).

634 The position of zebrafish during each trail was tracked using a published python package *Stytra* (Štih
635 et al., 2019). Using custom MATLAB algorithms, we calculated the overall angular movement of
636 zebrafish in the direction of the rotating grating for each trial as the optomotor index (OMI). For each
637 fish, OMI at a spatial frequency was averaged from results of 4 trials (2 repeats at either clockwise or
638 counter-clockwise direction). 5 dpf OMI data were normalized to the averaged OMI of *efemp1*$^{+/+}$ fish
639 at 0.0155 c/° (i.e., the condition for which 5 dpf zebrafish showed the greatest response) and 2 wpf OMI
640 data were normalized to averaged OMI of *efemp1*$^{+/+}$ fish at 0.0620 c/° (i.e., the condition for which 2
641 wpf zebrafish showed the greatest response). The spatial-frequency tuning functions were fit using a
642 log-Gaussian using a least-squares criterion to return amplitude (i.e., height of the peak), peak spatial
643 frequency (i.e., spatial frequency at which amplitude peaked), and bandwidth (i.e., standard deviation).

644 To test whether spatial-frequency tuning functions differed between groups, an omnibus *F*-test was
645 used to compare the goodness of fit (r^2) of a full model, in which parameter estimates of each group
646 could vary independently, with that of a restricted model, in which parameters were constrained to be

647 the same across groups. To determine whether specific parameter estimates differed between groups, a
648 nested *F*-test was used to compare a full model with a restricted model in which one parameter was
649 constrained to be the same across groups (Lu and Dosher, 2013). A criterion of $\alpha = 0.05$ was used to
650 determine significance.

651

652 **Optical coherence tomography (OCT)**

653 OCT was performed immediately after zebrafish were humanely killed using 1000 ppm AQUI-S
654 (#106036, Primo Aquaculture) in E3 medium. Zebrafish were positioned on a square (2 × 2 cm) of
655 paper towel and transferred onto a moistened PVA sponge fitted snugly in a 35-mm Petri dish. All OCT
656 images were recorded using a spectral domain OCT/OCTA system (Spectralis OCT2; Heidelberg
657 Engineering, Heidelberg, Germany) with the aid of a Digital High Mag lens (78D, Volk Optical Inc.,
658 Mentor, Ohio, USA) attached. The Petri dish was then affixed vertically onto a platform, allowing the
659 zebrafish eye to be aligned with the lens. Surface tension between the moistened sponge/paper towel
660 and the fish kept it in place. Images were acquired in the dorsal-ventral direction with a volume scan
661 pattern of 15° × 5° (2.7 × 0.9 mm). Each volume consisted of 128 B-scans (5 repeats) each consisting
662 of 512 A-scans. When imaging, the OCT was positioned such that the iris was horizontal, and a bright
663 reflection can be seen at the apex of the cornea. This ensured that the image captured was aligned with
664 the central axis of the eye. As myopia can independently develop in an eye without signals from the
665 brain (Troilo et al., 1987), and thus the other eye, both eyes were imaged for each zebrafish in our study.

666 Only for 5-dpf fish, eyes were imaged using a Bioptigen Envisu R2200 spectral domain OCT system
667 with an 18-mm telecentric lens (Bioptigen Inc., Durham, NC), due to temporary unavailability of the
668 Spectralis OCT system. The position of the sponge platform with a zebrafish (as described above) was
669 carefully adjusted to ensure that the central apex was aligned with the objective lens. A volume scan of
670 2 × 2 mm was acquired with a depth of 1.7 mm (1000 A-scans per B-scans).

671 Image quantification was performed using a custom MATLAB script. Axial length is quantified as the
672 distance from the corneal apex to the retinal pigment epithelium (RPE). Lens radius is half of the
673 distance from the anterior to posterior lens surface. The retinal radius is the distance from the center of

674 the lens to the RPE, which indeed can be calculated as the difference between axial length and lens
675 radius (Fig 2A). With these parameters, relative axial ocular refraction is given by the ratio of retinal
676 radius to lens radius (*Matthiessen's Ratio*), which is commonly used for analyzing ocular refraction of
677 aquatic species (Collery et al., 2014; Shand et al., 1999; Turnbull et al., 2015). *Two*- or *three*-way
678 ANOVA with Fisher's LSD tests were performed in Prism 9 (GraphPad, San Diego, CA, USA) and a
679 criterion of $\alpha = 0.05$ was used to determine statistical significance.

680

681 **Survival comparison between *efemp1*$^{2C\text{-}Cas9}$ fish with different eGFP levels**

682 *Efemp1*$^{2C\text{-}Cas9}$ fish were sorted under a fluorescence microscope and divided to two groups based on the
683 intensity of the retinal eGFP fluorescence; fish with weak eGFP signals were classified to eGFP+ group
684 and those with strong eGFP fluorescence were categorized to the eGFP+++ group. Both groups were
685 reared under standard husbandry and their survival was recorded at 2, 4, 6 and 8 weeks of age. There
686 were 3 tanks for both groups (37–60 fish each tank at 5 dpf). *Two*-way ANOVA and Fisher's LSD *post-*
687 *hoc* analyses were performed in Prism 9. A criterion of $\alpha = 0.05$ was used to determine significance.

688

689 **Electroretinography (ERG)**

690 The procedure for scotopic ERG was adapted from our published method (Xie et al., 2019c). Fish were
691 dark adapted (>8 hours, overnight) prior to experiments. All procedures were conducted under dim red
692 illumination (17.4 $cd \cdot m^{-2}$; $\lambda max = 600$ nm). For recording, a fish was humanely killed by immersing in
693 0.1% tricaine MS-222 (E10521; Sigma-Aldrich, St. Louis, MO, USA) in E3 medium. When gills had
694 stopped moving and fish were unresponsive response to a gentle touch, the head was removed and
695 immediately rinsed in E3 medium. The eyes were quickly dissected using fine-tipped tweezers under a
696 dissecting microscope. A small incision was made around the central cornea for each eye to allow a
697 small amount of aqueous humor to flow out. This helps keep the recording electrode to stay moist,
698 increasing conductivity and minimizing noise. The dissected eyes were moistened with multiple drops
699 of E3 medium using a 3-mm Pasteur pipette. The eyes were then transferred onto a square of paper
700 towel (2 × 2 cm) on a moist polyvinyl alcohol (PVA) sponge platform in a Faraday cage. Both eyes

701 were measured at the same time. For recording from eyes at or older than 4 wpf, recording electrodes
702 were 0.3-mm chloride-electroplated silvers (99%). For younger eyes, a moistened cone-shape sponge
703 (tip diameter ~40 μm) was attached to the silver. Under a microscope, the recoding electrodes were
704 positioned to gently touch the central corneal apex, and the reference electrodes were inserted into the
705 sponge platform. After electrode placement, the Ganzfeld bowl was moved to cover the platform, and
706 the eyes were allowed to dark adapt for 3 minutes. ERG responses for each fish were recorded with
707 flash stimuli of –2.11, –0.81, 0.72, 1.89 and 2.48 to analyze the impact of *efemp1* modification on retinal
708 function during normal development, and at −0.83, 0.73 and 1.87 log $cd \cdot s \cdot m^{-2}$ for examining how
709 *efemp1* modification impact fish's retinal physiological changes in response to myopia-inducing dark-
710 rearing. For stimulus intensities at or lower than 0.73 log $cd \cdot s \cdot m^{-2}$, three repeats were measured with
711 an inter-flash interval of 15 seconds and there was a 30-second interval between intensities. For stimulus
712 intensities at or higher than 1.87 log $cd \cdot s \cdot m^{-2}$, a single response was measured with a 60-second re-
713 adaption to dark before the flash.

714 All experiments were performed between 9:00 AM and 7:00 PM at room temperature. Amplitudes of
715 the *a*- and *b*- waves were measured from baseline to the negative *a*-wave trough and from the negative
716 *a*-wave trough to the *b*-wave peak, respectively. Implicit times of the *a*- and *b*-waves were measured
717 from stimulus onset to the *a*-wave trough and the *b*-wave peak, respectively. *Two*- or *three*-way
718 ANOVA, and Fisher's LSD *post-hoc* tests were performed in Prism 9. A criterion of $\alpha = 0.05$ was used
719 to determine significance.

720

721 **Gene expression analysis**

722 Zebrafish were humanely killed by 1000 ppm AQUIS (#106036, Primo Aquaculture) and stored in
723 RNALater (AM7020, Thermo Fisher, Waltham, MA, USA) at –20°C if not immediately used for RNA
724 isolation. For RNA isolation, eyes were dissected from zebrafish and lenses were removed. For each
725 sample, the total RNA of 4 eyes from two fish was isolated using TRIzol (or TRI-reagent; AM9738,
726 Thermo Fisher scientific) (Rio et al., 2010) and quantified using a Nanodrop 1000 (Thermo Fisher
727 Scientific). 750 ng (2 days of treatment) or 1 μg (4 weeks of treatment) of the total RNA was reverse-

728 transcribed into cDNA using a Tetro cDNA synthesis kit (BIO-65042, Bioline). Quantitative PCR (RT-
729 qPCR) assays were performed on a CFX96 real-time PCR system (Bio-Rad, Hercules, CA, USA) using
730 SsoAdvanced Universal SYBR Green Supermix (12 µL final mix per reaction; 1725272, Bio-Rad). In
731 this study, mRNA levels of *egr1*, *efemp1*, *tgfb1a*, *tgfb1b*, *vegfaa*, *vegfab*, *igf1*, *fgf2*, *wnt1b*, *rbp3*, *gjd2a*
732 and *gjd2b* were quantified. Primers of the tested genes were as listed in our previous study (Xie et al.,
733 2023 Preprint). A housekeeping gene *elongation factor 1-alpha* (*ef1a*) served as an internal control
734 (McCurley and Callard, 2008). For each gene, there were 4 samples per group and 3 replicates per
735 sample. Calculation of expression levels was performed using the $2^{-\Delta\Delta CT}$ method (Livak and Schmittgen,
736 2001) and the transcript levels were normalized to the *ef1a* transcript levels in L/D-reared *efemp1*$^{+/+}$
737 eyes at each time point. For statistics, *two*-way ANOVA and Fisher's LSD *post-hoc* tests were
738 performed in Prism 9. A criterion of $\alpha = 0.05$ was used to determine significance.

739

740 **Histology**

741 For Immunohistochemistry, whole zebrafish (if at 2 weeks of age) or dissected zebrafish eyes (if older
742 than 2 weeks of age; lenses excluded) were fixed in 4% paraformaldehyde (PFA) in PBS for 48 hours
743 at 4°C. They were cryoprotected in 30% sucrose in PBS, embedded in Tissue-Tek OCT compound
744 (Sakura Finetek, Torrance, CA, US) and cryosectioned (20 µm of thickness; CM 1860 Cryostat; Leica,
745 Wetzlar, Germany). Antibody staining was carried out at room temperature using standard protocols.
746 Slides were blocked in 5% fetal bovine serum (FBS) for 30 minutes and incubated overnight in rabbit
747 anti-EFEMP1 (ARP41450_P050, 1:600; Sapphire Bioscience, NSW, Australia), sheep anti-TIMP2
748 (1:1000; kind gift from the Itoh Lab at the University of Oxford, UK) or rabbit anti-MMP2 (AS-55111,
749 1:250; AnaSpec, Fremont, CA, USA) primary antibodies diluted in FBS. Slides were subsequently
750 incubated for 2 hours in secondary antibodies (all 1:500; Thermo Fisher Scientific) diluted in FBS. The
751 secondary antibodies used were Chicken anti-Rabbit Alexa Fluor 647 (A21443) or Donkey anti-Sheep
752 Alexa Fluor 647 (A21448). Nuclei were counterstained with 4′ ,6-diamidino-2- phenylindole (DAPI;
753 D9542-10MG, 1:10000; Sigma-Aldrich) in PBS for 20 minutes, and sections were mounted in Mowiol
754 (81381-250G; Sigma-Aldrich). Stained sections were imaged at a distance 100 µm from the center of

755 the optic nerve, using a Nikon A1R confocal microscope (Nikon, Minato City, Tokyo, Japan) with a
756 40× air objective lens (NA 0.95). For all confocal imaging, the deconvolution function of the NIS
757 elements software (AR4.6, Nikon) was applied to minimize background noise. Image brightness and
758 contrast were adjusted using Photoshop (Adobe, San Jose, CA, USA) or FIJI (Schindelin et al., 2012).

759 To analyze the relative distribution of EFEMP1, TIMP2 and MMP2, images were pre-processed in FIJI.
760 In each image, an inner retinal region was selected by drawing a line that followed the contour of the
761 inner plexiform layer (IPL) with a line thickness of 1000 pixels, which includes the inner nuclear layer
762 (INL; including the amacrine cell layer, ACL), IPL and ganglion cell layer (GCL). This line allowed
763 the retinal cross section to be straightened using the 'Straighten' function. The duplicated images
764 returned were rotated, positioning the INL on the left and GCL on the right. The widths of the
765 straightened images were then resized using Adobe Photoshop to normalize the IPL thickness to the
766 averaged IPL thickness of the control group (L/D-reared *efemp1*$^{+/+}$ fish) relevant to that timepoint.
767 Regions of interest (ROI) boxes measuring 150-pixel height and widths of 390 (2-day L/D- or DD-
768 reared *efemp1*$^{+/+}$ and *efemp1*$^{2C\text{-}Cas9}$ fish) or 455 pixels (4-week L/D- or DD-reared *efemp1*$^{+/+}$ and
769 *efemp1*$^{2C\text{-}Cas9}$ fish) were used to return expression levels using the '*Plot Profile*' function in FIJI. For
770 each image, brightness profiles across the ACL, IPL and GCL were normalized to the highest value. To
771 examine relative change in the three layers, normalized intensity was summed throughout the ACL
772 (pixel 1–90), IPL (2-day: pixel 91–300; 4-week: pixel 91–330) and GCL (2-day: pixel 301–390; 4-week:
773 pixel 331–455) for each image. One section per retina was used and both eyes from a zebrafish were
774 taken for analysis in this study. *Two*-way ANOVA and Fisher's LSD *post-hoc* tests were performed in
775 Prism 9 and a criterion of $\alpha = 0.05$ was used to determine statistical significance.

776

777 **Data availability**

778 All data have been made available on Open Science Frame (https://osf.io/rdmvy/).

779

780

781 **Acknowledgments**

782 We thank Yoshi Itoh for his kind gift of a sheet anti-TIMP2 antibody and Dr. Mirana Ramialison for
783 providing the p*Tol2* plasmid. We thank the Biological Optical Microscopy Platform (BOMP) at the
784 University of Melbourne for providing instrument for confocal imaging. We acknowledge the staff of
785 the Danio rerio University of Melbourne, and Walter and Eliza Hall of Medical Institute fish facilities
786 for animal husbandry and support.

787 JX was supported by the Melbourne Research Scholarship for his PhD study the Dr Albert Shimmins
788 Postgraduate Writing-Up Award for manuscript preparation. Funding was provided through the
789 University of Melbourne research grant support scheme and an international collaborative fund from
790 Research Centre for SHARP vision (RCSV), The Hong Kong Polytechnic University.

791

792 **Author Contributions**

793 Conceptualization, JX, BVB, PTG, PJ; Methodology, JX, BVB, PTG, PJ; Data collection, JX; Writing
794 – Original Draft, JX; Writing – Review & Editing, JX, BVB, PJ; Data analysis and visualization, JX;
795 Supervision, BVB, PTG, PJ; Project Administration, PJ; Funding Acquisition, PJ.

796

797 **Disclosure and competing interests statement**

798 The authors declare no conflict of interest.

799 **References**

800 Albig, A.R., J.R. Neil, and W.P. Schiemann. 2006. Fibulins 3 and 5 Antagonize Tumor Angiogenesis In vivo.
801 *Cancer Res* 66:2621-2629 10.1158/0008-5472.Can-04-4096.
802 An, J., E. Hsi, X. Zhou, Y. Tao, S.-H.H. Juo, and C.-L. Liang. 2012. The FGF2 gene in a myopia animal model and
803 human subjects. *Molecular Vision* 18:471
804 Ashby, R.S., G. Zeng, A.J. Leotta, D.Y. Tse, and S.A. McFadden. 2014. Egr-1 mRNA Expression Is a Marker for the
805 Direction of Mammalian Ocular Growth. *Investigative Ophthalmology & Visual Science* 55:5911-5921
806 10.1167/iovs.13-11708.
807 Bikfalvi, A., S. Klein, G. Pintucci, and D.B. Rifkin. 1997. Biological Roles of Fibroblast Growth Factor-2*.
808 *Endocrine Reviews* 18:26-45 10.1210/edrv.18.1.0292.
809 Blomfield, A.K., M. Maurya, K. Bora, M.C. Pavlovich, F. Yemanyi, S. Huang, Z. Fu, A.E. O'Connell, and J. Chen.
810 2023. Ectopic Rod Photoreceptor Development in Mice with Genetic Deficiency of WNT2B. *Cells*
811 12:1033
812 Bloomfield, S.A., and B. Völgyi. 2009. The diverse functional roles and regulation of neuronal gap junctions in
813 the retina. *Nature Reviews Neuroscience* 10:495
814 Collantes, E.R.A., M.S. Delfin, B. Fan, J.M.R. Torregosa, C. Siguan-Bell, N.V.d.G. Florcruz, J.M.D. Martinez, B.J.
815 Masna-Hidalgo, V.P.T. Guzman, J.F. Anotado-Flores, F.D. Levina, S.R.C. Hernandez, A.A. Collantes, M.C.
816 Sibulo, S. Rong, and J.L. Wiggs. 2022. EFEMP1 rare variants cause familial juvenile-onset open-angle
817 glaucoma. *Human Mutation* 43:240-252 https://doi.org/10.1002/humu.24320.
818 Collery, R.F., K.N. Veth, A.M. Dubis, J. Carroll, and B.A. Link. 2014. Rapid, accurate, and non-invasive
819 measurement of zebrafish axial length and other eye dimensions using SD-OCT allows longitudinal
820 analysis of myopia and emmetropization. *PLoS One* 9:e110699
821 Crowley, M.A., D.L. Garland, H. Sellner, A. Banks, L. Fan, T. Rejtar, N. Buchanan, O. Delgado, Y.Y. Xu, S. Jose,
822 C.M. Adams, M. Mogi, K. Wang, C.E. Bigelow, S. Poor, K. Anderson, B.D. Jaffee, G. Prasanna, C.
823 Grosskreutz, R. Fernandez-Godino, E.A. Pierce, T.P. Dryja, and S.-M. Liao. 2022. Complement factor B
824 is critical for sub-RPE deposit accumulation in a model of Doyne honeycomb retinal dystrophy with
825 features of age-related macular degeneration. *Human Molecular Genetics* 32:204-217
826 10.1093/hmg/ddac187.
827 Daniel, S., M. Renwick, V.Q. Chau, S. Datta, P. Maddineni, G. Zode, E.M. Wade, S.P. Robertson, W.M. Petroll,
828 and J.D. Hulleman. 2020. Fibulin-3 knockout mice demonstrate corneal dysfunction but maintain
829 normal retinal integrity. *Journal of Molecular Medicine* 98:1639-1656 10.1007/s00109-020-01974-z.
830 Di Donato, V., F. De Santis, T.O. Auer, N. Testa, H. Sánchez-Iranzo, N. Mercader, J.-P. Concordet, and F. Del
831 Bene. 2016. 2C-Cas9: a versatile tool for clonal analysis of gene function. *Genome research* 26:681-
832 692
833 Ding, X., D. Fu, S. Ge, Q. Guan, M. Chen, and Z. Yu. 2020. DNA methylation and mRNA expression of IGF-1 and
834 MMP-2 after form-deprivation myopia in guinea pigs. *Ophthalmic and Physiological Optics* 40:491-501
835 https://doi.org/10.1111/opo.12696.
836 Driver, S.G.W., M.R. Jackson, K. Richter, P. Tomlinson, B. Brockway, B.J. Halliday, D.M. Markie, S.P. Robertson,
837 and E.M. Wade. 2020. Biallelic variants in EFEMP1 in a man with a pronounced connective tissue
838 phenotype. *European Journal of Human Genetics* 28:445-452 10.1038/s41431-019-0546-7.
839 Fischer, A.J., J.J. McGuire, F. Schaeffel, and W.K. Stell. 1999. Light- and focus-dependent expression of the
840 transcription factor ZENK in the chick retina. *Nature Neuroscience* 2:706-712 10.1038/11167.
841 Garland, D.L., R. Fernandez-Godino, I. Kaur, K.D. Speicher, J.M. Harnly, J.D. Lambris, D.W. Speicher, and E.A.
842 Pierce. 2013. Mouse genetics and proteomic analyses demonstrate a critical role for complement in a
843 model of DHRD/ML, an inherited macular degeneration. *Human Molecular Genetics* 23:52-68
844 10.1093/hmg/ddt395.
845 Gerber, D.M., F.L. Munier, and G.n. Niemeyer. 2003. Cross-sectional Study of Visual Acuity and
846 Electroretinogram in Two Types of Dominant Drusen. *Investigative Ophthalmology & Visual Science*
847 44:493-496 10.1167/iovs.01-0787.
848 Gonzalez-Fernandez, F., and D. Ghosh. 2008. Focus on molecules: interphotoreceptor retinoid-binding protein
849 (IRBP). *Experimental eye research* 86:169-170
850 Holden, B.A., T.R. Fricke, D.A. Wilson, M. Jong, K.S. Naidoo, P. Sankaridurg, T.Y. Wong, T.J. Naduvilath, and S.
851 Resnikoff. 2016. Global prevalence of myopia and high myopia and temporal trends from 2000
852 through 2050. *Ophthalmology* 123:1036-1042

Itoh, H., P. Keller, H. Mogami, A. Lindqvist, and R. Word. 2010. Progesterone and transforming growth factor beta 1 (TGFB1) regulate matrix metalloproteinases (MMPS) in human endometrium. *Fertility and Sterility* 94:S214

Jia, Y., D.-N. Hu, J. Sun, and J. Zhou. 2017. Correlations Between MMPs and TIMPs Levels in Aqueous Humor from High Myopia and Cataract Patients. *Current Eye Research* 42:600-603 10.1080/02713683.2016.1223317.

Jia, Y., D.-N. Hu, D. Zhu, L. Zhang, P. Gu, X. Fan, and J. Zhou. 2014. MMP-2, MMP-3, TIMP-1, TIMP-2, and TIMP-3 Protein Levels in Human Aqueous Humor: Relationship With Axial Length. *Investigative Ophthalmology & Visual Science* 55:3922-3928 10.1167/iovs.14-13983.

Jobling, A.I., M. Nguyen, A. Gentle, and N.A. McBrien. 2004. Isoform-specific changes in scleral transforming growth factor-β expression and the regulation of collagen synthesis during myopia progression. *Journal of Biological Chemistry* 279:18121-18126

Kleiner, M., D. Brainard, D. Pelli, A. Ingling, R. Murray, and C. Broussard. 2007. What's new in Psychtoolbox-3. *Perception* 36:1

Kroll, F., G.T. Powell, M. Ghosh, G. Gestri, P. Antinucci, T.J. Hearn, H. Tunbak, S. Lim, H.W. Dennis, J.M. Fernandez, D. Whitmore, E. Dreosti, S.W. Wilson, E.J. Hoffman, and J. Rihel. 2021. A simple and effective F0 knockout method for rapid screening of behaviour and other complex phenotypes. *eLife* 10:e59683 10.7554/eLife.59683.

Kuiper, E.J., J.M. Hughes, R.J. Van Geest, I.M.C. Vogels, R. Goldschmeding, C.J.F. Van Noorden, R.O. Schlingemann, and I. Klaassen. 2007. Effect of VEGF-A on Expression of Profibrotic Growth Factor and Extracellular Matrix Genes in the Retina. *Investigative Ophthalmology & Visual Science* 48:4267-4276 10.1167/iovs.06-0804.

Labun, K., T.G. Montague, M. Krause, Y.N. Torres Cleuren, H. Tjeldnes, and E. Valen. 2019. CHOPCHOP v3: expanding the CRISPR web toolbox beyond genome editing. *Nucleic acids research* 47:W171-W174

Liu, Y., and Y. Sun. 2018. MMP-2 participates in the sclera of guinea pig with form-deprivation myopia via IGF-1/STAT3 pathway. *European Review for Medical and Pharmacological Sciences* 22:2541-2548

Livak, K.J., and T.D. Schmittgen. 2001. Analysis of Relative Gene Expression Data Using Real-Time Quantitative PCR and the 2−ΔΔCT Method. *Methods* 25:402-408 https://doi.org/10.1006/meth.2001.1262.

Livingstone, I., V.N. Uversky, D. Furniss, and A. Wiberg. 2020. The Pathophysiological Significance of Fibulin-3. *Biomolecules* 10:1294

Lu, Z.-L., and B. Dosher. 2013. Visual psychophysics: From laboratory to theory. MIT Press,

Ma, M., Z. Zhang, E. Du, W. Zheng, Q. Gu, X. Xu, and B. Ke. 2014. Wnt signaling in form deprivation myopia of the mice retina. *PLoS One* 9:e91086

Mackenzie, F., and C. Ruhrberg. 2012. Diverse roles for VEGF-A in the nervous system. *Development* 139:1371-1380 10.1242/dev.072348.

Marmorstein, L.Y., F.L. Munier, Y. Arsenijevic, D.F. Schorderet, P.J. McLaughlin, D. Chung, E. Traboulsi, and A.D. Marmorstein. 2002. Aberrant accumulation of EFEMP1 underlies drusen formation in Malattia Leventinese and age-related macular degeneration. *Proceedings of the National Academy of Sciences* 99:13067-13072 doi:10.1073/pnas.202491599.

McCurley, A.T., and G.V. Callard. 2008. Characterization of housekeeping genes in zebrafish: male-female differences and effects of tissue type, developmental stage and chemical treatment. *BMC molecular biology* 9:1-12

Najafzadeh, M.J., A. Zand, M. Shafiei, M. Sharifi, N. Nasiri, and A. Sharifi. 2023. Myopia Progression during the COVID-19 Era: A Systematic Review and Meta-analysis. *Seminars in Ophthalmology* 1-10 10.1080/08820538.2023.2168490.

Quint, W.H., K.C. Tadema, E. de Vrieze, R.M. Lukowicz, S. Broekman, B.H. Winkelman, M. Hoevenaars, H.M. de Gruiter, E. Van Wijk, and F. Schaeffel. 2021. Loss of Gap Junction Delta-2 (GJD2) gene orthologs leads to refractive error in zebrafish. *Communications Biology* 4:676

Rabin, J., R.C. Van Sluyters, and R. Malach. 1981. Emmetropization: a vision-dependent phenomenon. *Investigative Ophthalmology & Visual Science* 20:561-564

Rio, D.C., M. Ares, G.J. Hannon, and T.W. Nilsen. 2010. Purification of RNA using TRIzol (TRI reagent). *Cold Spring Harbor Protocols* 2010:pdb. prot5439

Rose, K.A., I.G. Morgan, J. Ip, A. Kifley, S. Huynh, W. Smith, and P. Mitchell. 2008. Outdoor activity reduces the prevalence of myopia in children. *Ophthalmology* 115:1279-1285

Schindelin, J., I. Arganda-Carreras, E. Frise, V. Kaynig, M. Longair, T. Pietzsch, S. Preibisch, C. Rueden, S. Saalfeld, and B. Schmid. 2012. Fiji: an open-source platform for biological-image analysis. *Nature methods* 9:676

Schippert, R., E. Burkhardt, M. Feldkaemper, and F. Schaeffel. 2007. Relative Axial Myopia in Egr-1 (ZENK) Knockout Mice. *Investigative Ophthalmology & Visual Science* 48:11-17 10.1167/iovs.06-0851.

Seko, Y., H. Shimokawa, and T. Tokoro. 1995. Expression of bFGF and TGF-beta 2 in experimental myopia in chicks. *Investigative Ophthalmology & Visual Science* 36:1183-1187

Shand, J., K.B. Døving, and S.P. Collin. 1999. Optics of the developing fish eye: comparisons of Matthiessen's ratio and the focal length of the lens in the black bream Acanthopagrus butcheri (Sparidae, Teleostei). *Vision Research* 39:1071-1078 https://doi.org/10.1016/S0042-6989(98)00215-6.

Shi, W.-Q., T. Wan, B. Li, T. Li, and X.-D. Zhou. 2023. EFEMP1 is a potential biomarker of choroid thickness change in myopia. *Frontiers in Neuroscience* 17:1144421

Singh, V.K., A. Mangalam, S. Dwivedi, and S. Naik. 1998. Primer premier: program for design of degenerate primers from a protein sequence. *Biotechniques* 24:318-319

Štih, V., L. Petrucco, A.M. Kist, and R. Portugues. 2019. Stytra: An open-source, integrated system for stimulation, tracking and closed-loop behavioral experiments. *PLOS Computational Biology* 15:e1006699 10.1371/journal.pcbi.1006699.

Stone, E.M., A.J. Lotery, F.L. Munier, E. Héon, B. Piguet, R.H. Guymer, K. Vandenburgh, P. Cousin, D. Nishimura, R.E. Swiderski, G. Silvestri, D.A. Mackey, G.S. Hageman, A.C. Bird, V.C. Sheffield, and D.F. Schorderet. 1999. A single EFEMP1 mutation associated with both Malattia Leventinese and Doyne honeycomb retinal dystrophy. *Nature Genetics* 22:199-202 10.1038/9722.

Stratikopoulos, E., M. Szabolcs, I. Dragatsis, A. Klinakis, and A. Efstratiadis. 2008. The hormonal action of IGF1 in postnatal mouse growth. *Proceedings of the National Academy of Sciences* 105:19378-19383 doi:10.1073/pnas.0809223105.

Tedja, M.S., A.E.G. Haarman, M.A. Meester-Smoor, J. Kaprio, D.A. Mackey, J.A. Guggenheim, C.J. Hammond, V.J.M. Verhoeven, C.C.W. Klaver, and f.t.C. Consortium. 2019. IMI – Myopia Genetics Report. *Investigative Ophthalmology & Visual Science* 60:M89-M105 10.1167/iovs.18-25965.

Tedja, M.S., R. Wojciechowski, P.G. Hysi, N. Eriksson, N.A. Furlotte, V.J. Verhoeven, A.I. Iglesias, M.A. Meester-Smoor, S.W. Tompson, and Q. Fan. 2018. Genome-wide association meta-analysis highlights light-induced signaling as a driver for refractive error. *Nature genetics* 50:834

Troilo, D., M.D. Gottlieb, and J. Wallman. 1987. Visual deprivation causes myopia in chicks with optic nerve section. *Current eye research* 6:993-999

Turnbull, P.R.K., S. Backhouse, and J.R. Phillips. 2015. Visually guided eye growth in the squid. *Current Biology* 25:R791-R792 10.1016/j.cub.2015.07.073.

Wallman, J., M.D. Gottlieb, V. Rajaram, and L.A. Fugate-Wentzek. 1987. Local retinal regions control local eye growth and myopia. *Science* 237:73-77

Wisard, J., A. Faulkner, M.A. Chrenek, T. Waxweiler, W. Waxweiler, C. Donmoyer, G.I. Liou, C.M. Craft, G.F. Schmid, J.H. Boatright, M.T. Pardue, and J.M. Nickerson. 2011. Exaggerated Eye Growth in IRBP-Deficient Mice in Early Development. *Investigative Ophthalmology & Visual Science* 52:5804-5811 10.1167/iovs.10-7129.

Xie, J., P.T. Goodbourn, B.V. Bui, and P.R. Jusuf. 2023. Establishment and comprehensive characterization of a novel dark-reared zebrafish model for myopia studies. *bioRxiv* doi.org/10.1101/2023.11.19.567749 (Preprint posted November 21, 2023).

Xie, J., P.T. Goodbourn, B.V. Bui, T.E. Sztal, and P.R. Jusuf. 2019a. Correspondence Between Behavioral, Physiological, and Anatomical Measurements of Visual Function in Inhibitory Neuron–Ablated Zebrafish. *Investigative ophthalmology & visual science* 60:4681-4690

Xie, J., P.R. Jusuf, B.V. Bui, S. Dudczig, T.E. Sztal, and P.T. Goodbourn. 2021. Altered Visual Function in a Larval Zebrafish Knockout of Neurodevelopmental Risk Gene pdzk1. *Investigative Ophthalmology & Visual Science* 62:29-29 10.1167/iovs.62.3.29.

Xie, J., P.R. Jusuf, B.V. Bui, and P.T. Goodbourn. 2019b. Experience-dependent development of visual sensitivity in larval zebrafish. *Scientific Reports* 9:1-11

Xie, J., P.R. Jusuf, P.T. Goodbourn, and B.V. Bui. 2019c. Electroretinogram Recording in Larval Zebrafish using A Novel Cone-Shaped Sponge-tip Electrode. *JoVE* e59487 10.3791/59487.

Yang, T., H. Zhang, H. Qiu, B. Li, J. Wang, G. Du, C. Ren, and X. Wan. 2016. EFEMP1 is repressed by estrogen and inhibits the epithelial-mesenchymal transition via Wnt/β-catenin signaling in endometrial carcinoma. *Oncotarget* 7:25712

Yue, B. 2014. Biology of the extracellular matrix: an overview. *Journal of glaucoma* S20

Zhu, X., S. Dellostritto, A. Nour, and A. Benavente-Perez. 2021. Vascular Endothelial Growth Factor-A (VEGF-A) and High Myopia in Marmosets. *Investigative Ophthalmology & Visual Science* 62:2875-2875